

1 **Title:** A naturally arising broad and potent CD4-binding site antibody with low somatic mutation

2 **Short Title:** An HIV-1 bNAb with low somatic mutation

3

4 **Authors**

5 Christopher O. Barnes<sup>1,†,‡</sup>, Till Schoofs<sup>2,3,4,†,§</sup>, Priyanthi N.P. Gnanapragasam<sup>1</sup>, Jovana Golijanin<sup>2</sup>,

6 Kathryn E. Huey-Tubman<sup>1</sup>, Henning Gruell<sup>3,4</sup>, Philipp Schommers<sup>3,4,5</sup>, Nina Suh-Toma<sup>1</sup>, Yu Erica

7 Lee<sup>1</sup>, Julio C. Cetrulo Lorenzi<sup>2,||</sup>, Alicja Piechocka-Trocha<sup>6</sup>, Johannes F. Scheid<sup>7</sup>, Anthony P.

8 West, Jr<sup>1</sup>, Bruce D. Walker<sup>6,8</sup>, Michael S. Seaman<sup>9</sup>, Florian Klein<sup>3,4,10</sup>, Michel C. Nussenzweig<sup>2,8\*</sup>,

9 Pamela J. Bjorkman<sup>1\*</sup>

10

11 **Affiliations**

12 <sup>1</sup>Division of Biology and Biological Engineering, California Institute of Technology, Pasadena,

13 CA 91125, USA

14 <sup>2</sup>Laboratory of Molecular Immunology, The Rockefeller University, New York, NY 10065, USA

15 <sup>3</sup>Laboratory of Experimental Immunology, Institute of Virology, University of Cologne, Faculty

16 of Medicine and University Hospital of Cologne, University of Cologne, 50931 Cologne,

17 Germany

18 <sup>4</sup>German Center for Infection Research, partner site Bonn–Cologne, 50931 Cologne, Germany

19 <sup>5</sup>Department I of Internal Medicine, Faculty of Medicine and University Hospital Cologne,

20 University of Cologne, 50931 Cologne, Germany

21 <sup>6</sup>Ragon Institute of Massachusetts General Hospital, Massachusetts Institute of Technology and

22 Harvard University, Cambridge, MA 02129, USA

23 <sup>7</sup>Division of Gastroenterology, Massachusetts General Hospital, Boston 02114, USA

24 <sup>8</sup>Howard Hughes Medical Institute, Chevy Chase, MD 20815, USA

25 <sup>9</sup>Center for Virology and Vaccine Research, Beth Israel Deaconess Medical Center, Harvard  
26 Medical School, Boston, MA 02215, USA

27 <sup>10</sup>Center for Molecular Medicine Cologne (CMMC), University of Cologne, 50931 Cologne,  
28 Germany

29

30 †These authors contributed equally

31 ‡Present address: Department of Biology, Stanford University, Stanford, CA, 94305, USA

32 §Present address: GSK Vaccines, 1330 Rixensart, Belgium

33 ||Present address: Moderna Therapeutics, 200 Tech Square, Cambridge, MA, 02142, USA

34

35 \*Correspondence should be addressed to: Michel C. Nussenzweig ([nussen@rockefeller.edu](mailto:nussen@rockefeller.edu)) and

36 Pamela J. Bjorkman ([bjorkman@caltech.edu](mailto:bjorkman@caltech.edu))

37

38

39 **Abstract**

40 The induction of broadly neutralizing antibodies (bNAbs) is a potential strategy for a vaccine  
41 against HIV-1. However, most bNAbs exhibit features such as unusually high somatic  
42 hypermutation, including insertions and deletions, which make their induction challenging.  
43 VRC01-class bNAbs exhibit extraordinary breadth and potency, but also rank among the most  
44 highly somatically-mutated bNAbs. Here we describe a VRC01-class antibody isolated from a  
45 viremic controller, BG24, that has less than half the mutations of most other relatives of its class,  
46 while achieving comparable breadth and potency. A 3.8 Å X-ray crystal structure of a BG24-  
47 BG505 Env trimer complex revealed conserved contacts at the gp120 interface characteristic of  
48 the VRC01-class Abs, despite lacking common CDR3 sequence motifs. The existence of  
49 moderately-mutated CD4-binding site (CD4bs) bNAbs such as BG24 provides a simpler blueprint  
50 for CD4bs antibody induction by a vaccine, raising the prospect that such an induction might be  
51 feasible with a germline-targeting approach.

52

53 **Teaser:**

54 An anti-HIV-1 antibody with comparable neutralization breadth and potency to similarly-classed  
55 antibodies, with half as many mutations.

56

57

58 **MAIN TEXT**

59 **Introduction**

60 In the last decade, it was discovered that a subset of HIV-1–infected individuals produce potent  
61 and broadly neutralizing antibodies (bNAbs) that target the HIV-1 envelope protein (Env) (*1-10*),  
62 a trimeric spike of gp120-gp41 heterodimers on the viral surface. Potent bNAb epitopes have been  
63 mapped across the entire surface of Env (*11-16*), have been shown to protect against and suppress  
64 infection in animal models (*17-20*), and exhibit antiviral activity in human clinical trials against  
65 circulating viral clades (*21-24*). Thus, it has been hypothesized that bNAbs could provide  
66 protection from HIV-1 infection if an efficient means of eliciting such antibodies could be  
67 developed (*25, 26*). However, while potent autologous neutralizing antibodies and neutralizing  
68 antibodies with intermediate breadth have been induced in wild type animal models (*27-30*),  
69 immunization strategies have yet to elicit potent, heterologous neutralizing bNAbs. Unusual  
70 features of HIV-1 bNAbs are considered one of the main barriers to their induction (*31*). Such  
71 features include high levels of somatic mutation, long heavy chain complementarity determining  
72 region 3 (CDRH3) loops, and insertions or deletions in antibody variable regions, all of which are  
73 rare features in the human repertoire and do not usually emerge until one to three years post-  
74 infection (*7, 32*).

75

76 Historically, CD4-binding site bNAbs are among the most broad and potent bNAbs (*33-35*).  
77 Members of the VRC01-class of CD4-binding site bNAbs, characterized by IGVH1-2\*02 variable  
78 heavy (VH) gene segment use and an unusually short five-residue CDRL3 loop, have been isolated  
79 from many different donors and revealed to bind with a very similar orientation at the gp120  
80 interface (*36*). However, these bNAbs are among the most heavily somatically mutated, creating

81 a large barrier for induction of these antibodies in immunization strategies. Rational design has  
82 identified a minimally mutated version of VRC01-class antibodies that retains significant  
83 neutralization breadth and potency (37). However, it has been unclear whether such minimally  
84 mutated VRC01-class antibodies could arise naturally. Recently, a first example of a naturally-  
85 arising VRC01-class bNAb with a low mutation rate was described (38). The PCIN63 lineage  
86 showed similar features to VRC01-class bNAbs despite only 12-15% nucleotide somatic mutation  
87 compared to the putative germline V genes, providing evidence to a faster maturation route for  
88 VRC01-class bNAbs, where binding to the N276<sub>gp120</sub>-glycan may be an important first step and  
89 should be a consideration in VRC01-class priming immunogens.

90

91 Here, we describe antibody BG24, a VRC01-class bNAb, that targets the CD4-binding site with  
92 comparable neutralization breadth and potency to VRC01, while exhibiting half as many somatic  
93 mutations. We report CDR3 sequence motifs utilized by the BG24 lineage that are uncommon  
94 among VRC01-class bNAbs, challenging the notion of signature residues necessary for broad and  
95 potent neutralization. A 3.8Å crystal structure of BG24 Fab bound to a fully- and natively-  
96 glycosylated BG505 SOSIP.664 Env trimer (39) revealed a binding orientation consistent with  
97 VRC01-class bNAbs and contacts with an adjacent gp120 protomer. Collectively, these data  
98 provided the framework for engineering a minimally-mutated BG24 construct, which maintained  
99 breadth of binding to the mature construct and has direct implications in current HIV-1  
100 immunization strategies.

101

## 102 **Results**

### 103 **A family of VRC01-class antibodies in donor 391370 isolated by BG505-sorting**

104 Donor 391370 was first diagnosed with HIV-1 in 1990 and was followed as part of the HIV  
105 Controller Consortium from 2005-2008 (40). The subject's plasma from 2008 was previously  
106 tested against an early HIV-1 pseudovirus panel, showing broad and potent neutralizing activity  
107 (Table S1) (9, 41). To determine the epitope-specificity of 391370's serum neutralizing activity,  
108 neutralization fingerprinting was done using the f61 pseudovirus panel (42) on a purified IgG  
109 sample from 2007, which showed a VRC01-class neutralization fingerprint (Fig. 1A,B). Indeed, a  
110 direct comparison with purified IgG of Patient 3, the subject from whom 3BNC117 (9, 43) was  
111 isolated, confirmed a very similar neutralization profile in breadth, potency and fingerprinting (Fig.  
112 1A,B).

113         Due to strong neutralizing activity against BG505.T332N, single B cell sorting was carried  
114 out using BG505.SOSIP.664 (39) as a bait on a contemporaneous PBMC sample from 2007 (Fig.  
115 1C,D) as described (44). From 20 million PBMCs, we recovered a total of 152 heavy chain and  
116 159 light chain sequences from IgG<sup>+</sup> memory B-cells (Fig. S1A). Both heavy and light chain  
117 sequences were highly clonal with 68% and 58% of sequences belonging to expanded groups of  $\geq$   
118 2 clonally related members (Fig. S1A). Consistent with the VRC01-class fingerprint, the largest  
119 expanded clone was derived from an IGVH1-2\*02 heavy chain germline gene segment. However,  
120 in contrast to the majority of VRC01-class antibodies, the members utilized a lambda and not a  
121 kappa light chain that was derived from the germline IGLV2-11\*01 gene segment but showed the  
122 typical 5 amino acid length restriction in CDRL3 (Table S2).

123         Members of the IGVH1-2\*02/IGLV2-11\*01 clone showed quite a diverse phylogeny, but  
124 generally ranked lower in mutation count than other VRC01-class antibodies such as 3BNC117  
125 and VRC01 (Table S2, Fig. S1B,C). Following production of monoclonal antibodies from 25  
126 distinct members, we analyzed HIV-1 neutralizing activity against 5 viruses of the f61 panel that

127 were best neutralized by 391370's IgG (Fig. S1C). Clonal members exhibited a range of  
128 neutralization activity, and four members (BG5, BG24, BG33, BG38) with broad and potent anti-  
129 HIV activity were further tested on additional viruses of the f61 panel (Fig. S1D).

130 Clone member BG24 showed the most broad and potent neutralization activity, which  
131 recapitulated the serum neutralization profile of 391370's IgGs with a strong CD4-binding site  
132 fingerprint (Fig. S1D). Consistent with this fingerprint, BG24 showed a mutational sensitivity  
133 profile similar to VRC01-class antibodies when tested against a HIV<sub>YU2</sub> pseudovirus panel  
134 comprising escape mutations in common bNAb epitopes (Fig. S1E). Additional testing against the  
135 12-virus global panel (45) showed BG24 to have comparable neutralization breadth to VRC01 and  
136 3BNC117 (Fig. S1F). Moreover, BG24 exhibited equivalent breadth and potency to VRC01  
137 against a 126-virus panel representative of all major circulating HIV-1 clades, neutralizing 85% of  
138 viruses with a geometric mean IC<sub>50</sub> of 0.29 µg/ml (Fig. 1E, Table S3). As such, BG24 ranks among  
139 the most broad and potent of previously-described VRC01-class antibodies (Fig. 1E).

140 Surprisingly, BG24 showed one of the lowest numbers of somatic hypermutations of the  
141 clonal family, exhibiting 13.4% nucleotide (22.7% amino acid) and 8% nucleotide (19.5% amino  
142 acid) mutations in heavy and light chains, respectively. This mutation count is more than 2-fold  
143 lower than other VRC01-class antibodies (Fig. 1F, Fig. S2A, Table S2). In contrast to bNAbs 2F5  
144 and 4E10 (46), no autoreactivity was found for BG24 by HEp-2 staining (Fig. S2B). To date, only  
145 one other patient-derived VRC01-class antibody (PCIN71I) with similar breadth, potency and low  
146 mutational count has been described (38). The discovery and characterization of BG24 and related  
147 modestly mutated CD4bs bNAbs suggests that targeting of this epitope may not require a high  
148 level of mutations to achieve breadth and potency.

149

150 **BG24 displays sequence features atypical of VRC01-class bNAbs**

151 When aligned with other members of the VRC01-class bNAbs (Fig. S3A), BG24 shows  
152 conservation of sequence features such as R71<sub>HC</sub>, W50<sub>HC</sub>, N58<sub>HC</sub>, E96<sub>LC</sub> and a deletion in CDRL1  
153 to accommodate the gp120 N276-glycan (36). However, BG24 features a tyrosine at the -5 position  
154 in its CDRH3, a fixed position at the end of CDRH3 typically occupied by a tryptophan residue  
155 (36), and an uncommon 5-amino acid CDRL3 “SAFEY” sequence motif. Moreover, the presence  
156 of a potential N-linked glycosylation site (PNGS) at residue N58<sub>HC</sub>, which sits directly at the  
157 antigen-antibody interface, may alter BG24’s orientation at the CD4bs relative to other VRC01-  
158 class antibodies or reduce BG24’s ability to neutralize HIV-1 isolates.

159         Given that the Env binding orientations of VH1-2/VRC01-class bNAbs are highly  
160 convergent (12, 33, 36, 47), we speculated that glycosylation at position N58<sub>HC</sub> of BG24 would  
161 likely reduce its potency and breadth. Previous studies of glycosylation patterns in eukaryotic  
162 proteins have shown that the presence of a N-x-S/T sequon is necessary but not sufficient for  
163 glycosylation, and moreover, that the N-x-S sequon is less frequently glycosylated than the N-x-T  
164 sequon (48, 49). Thus, to assess the impact of N58<sub>HC</sub> glycosylation, we compared the neutralizing  
165 activity of a glycan-knockout construct (BG24 S60A<sub>HC</sub>) and a “glycan-occupied” construct (BG24  
166 S60T<sub>HC</sub>) to the wild-type protein on the DeCamp global 12-strain panel (45). While we observed  
167 no significant difference in the neutralizing activity between the wild-type and BG24 S60A<sub>HC</sub>  
168 construct, we observed an approximate 10-fold reduction in neutralization potency for the BG24  
169 S60T<sub>HC</sub> construct relative to wild-type (Fig. S3B). This result suggests that: i) the BG24 S60T<sub>HC</sub>  
170 construct has a higher N-glycan occupancy at position N58<sub>HC</sub> relative to wild-type BG24, and ii)  
171 glycosylation at position N58<sub>HC</sub> is positively correlated with reduced BG24 neutralizing activity,

172 which is likely explained by BG24 adopting a similar Env binding orientation as other VRC01-  
173 class bNAbs.

174

### 175 **Structure of BG24-Env complex shows similar recognition of gp120 as VRC01-class bNAbs**

176 Since we observed no difference in the neutralization profile of BG24 S60A<sub>HC</sub> compared to wild-  
177 type, we used the S60A<sub>HC</sub> construct to define the Env binding mechanism of BG24 to eliminate  
178 potential interference of a glycosylated N58<sub>HC</sub> residue in structural studies. We determined a 2.0  
179 Å crystal structure of the BG24 S60A<sub>HC</sub> Fab and a 3.8 Å crystal structure of BG24 S60A<sub>HC</sub> Fab in  
180 complex with a natively-glycosylated clade A BG505 SOSIP.664 trimer and a Fab from the V3-  
181 glycan targeting bNAb 10-1074 (Table S4 and Fig. 2A). Comparison of the BG24 Fab components  
182 of the two structures revealed that BG24 did not undergo large conformational changes upon Env  
183 binding (Fig. S4A, root mean square deviation of 0.9 Å when aligned against 219 C $\alpha$  atoms  
184 comprising the BG24 variable domains). Relative to VRC01-class bNAbs, BG24 maintained a  
185 similar gp120-binding orientation, consistent with an overall epitope focused on the portion of the  
186 CD4bs within the gp120 outer domain, framed by the N197<sub>gp120</sub>, N276<sub>gp120</sub>, and N363<sub>gp120</sub> glycans  
187 (Figs. 2B and S4B). With the exception of CDRL2, all BG24 CDRs were involved in gp120  
188 recognition, burying a similar degree of surface area on the CD4bs loop, D loop, and the V5-loop  
189 of gp120 as VRC01, VRC03 and 3BNC117 (Fig. S4C,D). Typical interactions between VRC01-  
190 class bNAbs and gp120 are conserved with BG24 including: i) a salt bridge between R71<sub>HC</sub> and  
191 D368<sub>gp120</sub>, ii) potential hydrogen bonding between W50<sub>HC</sub> and N280<sub>gp120</sub>, and iii) potential  
192 hydrogen bonding between N58<sub>HC</sub> and the backbone carbonyl of R456<sub>gp120</sub> (Fig. 2C).

193 In addition to the characteristic VH1-2 contacts, the BG24 epitope includes interprotomer  
194 interactions that have been observed for other VRC01-class antibodies (Fig. S4C,D)(50, 51).

195 However, unlike 3BNC117 or VRC03, which utilize insertions in HC FWR3 to contact the V3-  
196 loop base on the adjacent protomer (50, 52), BG24's CDRH1 interacts with  $\alpha 0$  residues of the  
197 adjacent gp120 protomer, with N28<sub>HC</sub> potentially hydrogen bonding with the backbone carbonyl  
198 of E64<sub>gp120</sub> (Fig. 4E). Moreover, BG24's binding orientation brings HC FWR1 into close proximity  
199 with the neighboring N301<sub>gp120</sub> glycan (modeled in the density as a complex-type biantennary N-  
200 glycan) burying  $\sim 127 \text{ \AA}^2$  of glycan surface area (Fig. S5A,B). This interaction is not unique to  
201 BG24, having been observed in crystal structures of a VRC01-bound high-mannose fully-  
202 glycosylated Env trimer (53) and an IOMA-bound natively- and fully-glycosylated Env trimer  
203 (12). However, in contrast to previous studies that attributed a shift to more positively-charged  
204 antigen combining sites of VRC01-class bNAbs to interactions with complex-type N-glycans (47),  
205 comparison of the N301<sub>gp120</sub> glycan binding surface on BG24 relative to germline VRC01 showed  
206 minimal changes in the electrostatic surface potential (Fig. S5C-E). This result suggests that unlike  
207 the complex-type N197<sub>gp120</sub> and N276<sub>gp120</sub> glycans that frame the CD4bs, the complex-type  
208 N301<sub>gp120</sub> glycan plays little to no role in VRC01-class bNAb maturation.

209

### 210 **Non-traditional CDR3 sequence motifs favorably interact with HIV-1 gp120**

211 In addition to low numbers of somatic mutations, BG24 is defined by CDR3 features that are  
212 uncommon among the VRC01-class antibodies. BG24 utilizes a 5-amino acid length CDRL3 with  
213 an unusual "SAFEY" sequence motif that differs from the consensus "QQYEF" motif of  $\kappa^+$   
214 VRC01-class bNAbs and is distinct among  $\lambda^+$  VRC01-class bNAbs (Fig. S3A) (36, 54). Despite  
215 the distinct CDRL3 sequence motif, BG24 includes a negatively-charged Glu residue at LC  
216 position 96 that maintains signature H-bond interactions with N280<sub>gp120</sub> and G459<sub>gp120</sub> in the D-  
217 and V5-loops, respectively (Fig. 3A). Additionally, E96<sub>LC</sub> potentially interacts with R456<sub>gp120</sub>, a

218 contact not routinely found in VRC01-class antibody-Env structures and only previously observed  
219 in an IOMA-BG505 Env structure due to IOMA's 8-residue CDRL3 (12).

220 In the heavy chain, BG24 lacks the canonical Trp residue at the -5 position in its CDRH3,  
221 which is highly-conserved in most VRC01-class antibodies and forms H-bond interactions with  
222 residue N279<sub>gp120</sub> at that antibody-antigen interface (36). Interestingly, enrichment of non-Trp  
223 residues at the -5 position of CDRH3 in naïve B-cells sorted with eOD-GT8, a VRC01-class  
224 targeting immunogen (55, 56), suggested that recombination of the CDRH3 with the low frequency  
225 IGHJ2\*01 gene segment is not a requirement of VRC01-class B-cell precursors, and a Trp residue  
226 in this position could plausibly arise during affinity maturation (54). BG24 features a Tyr at this  
227 position, which preserves D-loop interactions at the interface by forming a H-bond with a side  
228 chain oxygen atom on N280<sub>gp120</sub> (Fig. 3B). To test whether BG24 would show increased anti-HIV  
229 activity with a Trp residue in this position (Kabat numbering - CDRH3 residue 100D), we  
230 generated a Y100<sub>D</sub>W construct and assayed neutralizing activity against a 126 virus panel. We  
231 observed BG24 Y100<sub>D</sub> to be broader and more potent than BG24 W100<sub>D</sub>, as well as all other  
232 VRC01-class bNAbs lacking a Trp residue at the -5 position in CDRH3 (Fig. 3C,D and Table S3).  
233 Thus, our results demonstrate the potential for potency and breadth of VRC01-class antibodies  
234 encoding for non-Trp residues at this position, which is frequently observed in naïve B-cells sorted  
235 with CD4bs immunogens (54).

236

### 237 **Substitutions in BG24 CDRH2 loop improve neutralizing activity**

238 Previous studies have shown that VRC01-class antibody contacts with the gp120 inner domain  
239 (57), "Phe43 pocket" (58-60), or interprotomer interactions (51, 52) enhance antibody activity.  
240 Given BG24's low number of mutations, we sought to enhance BG24's potent neutralization and

241 breadth by incorporating substitutions in CDRH2 residues that mimic Phe43 pocket filling. In  
242 addition to the G54W mutation that was engineered into the VRC01-class bNAbs NIH45-46 and  
243 VRC07 (58, 60), we designed BG24 constructs that substituted CDRH2 residues from VRC-PG20  
244 (Fig. S6A), a IGVH1-2\*02 VRC01-class antibody that utilizes a  $\lambda^+$  light chain (IGVL2-14) and  
245 encodes a W54 residue in CDRH2 (61). We postulated that residues flanking the large aromatic  
246 substitution at position 54 potentially reduce polyreactive recognition of non-HIV-1 antigens  
247 previously observed for the G54W substitution (62). To assess potential polyreactivity of BG24  
248 and the BG24-derived constructs, we utilized a baculovirus-based polyreactivity assay (63). While  
249 antibodies NIH45-46<sup>G54W</sup>, 2F5 and 4E10, (which are known to be polyreactive) showed strong  
250 signals, no evidence of polyreactivity was found for BG24 or any of the designed constructs (Fig.  
251 S6B).

252 We next tested our constructs for neutralizing activity on the 12-strain global panel (45)  
253 and compared potency and breadth against BG24. In general, we observed a 2-5-fold improvement  
254 in IC<sub>50</sub> values for all constructs relative to unmodified BG24, with constructs containing VRC-  
255 PG20 CDRH2 sequences being the most potent (Fig. 4A). When tested against a 126 virus panel,  
256 the engineered BG24 constructs achieved ~90% breadth and a 2-3 fold improvement in the  
257 geometric mean IC<sub>50</sub> value relative to BG24 (Table S3: BG24 – IC<sub>50</sub>=0.29 $\mu$ g/mL / 84.9% breadth;  
258 BG24<sub>G54W</sub> – IC<sub>50</sub>=0.15 $\mu$ g/mL / 88.1% breadth; BG24<sub>PG20-CDR2-v1</sub> – IC<sub>50</sub>=0.15 $\mu$ g/mL / 92.9%  
259 breadth; BG24<sub>PG20-CDR2-v2</sub> – IC<sub>50</sub>=0.14 $\mu$ g/mL / 92.1% breadth).

260 To understand the basis of this increased neutralizing activity, we solved a 3.5 Å single-  
261 particle cryo-EM structure of a natively-glycosylated DU422 SOSIP.664 v4.1 trimer in complex  
262 with BG24<sub>PG20-CDR2-v2</sub> and 10-1074 Fabs (Fig.s 4B, S6C-F and Table S5). Consistent with previous  
263 observations(58, 60), the W54<sub>HC</sub> residue encoded by CDRH2 is accommodated within gp120's

264 Phe43 pocket, increasing contacts with the gp120 inner domain (Fig. 4C-E). Additionally, N53<sub>HC</sub>  
265 and N56<sub>HC</sub> form backbone potential backbone interactions with G469-G470<sub>gp120</sub> and R61<sub>HC</sub>  
266 establishes an additional salt bridge with E462<sub>gp120</sub>, interactions not observed with the parent BG24  
267 antibody. Collectively, these interactions add an additional  $\sim 170 \text{ \AA}^2$  of buried surface area on the  
268 antibody paratope by providing favorable interactions that likely increase BG24's affinity to the  
269 CD4bs epitope, explaining the enhanced neutralization activity of against DU422.

270

### 271 **BG24 has comparable *in vivo* efficacy to VRC01**

272 Anti-HIV-1 bNAbs are being considered as agents for HIV-1 treatment and prevention. A few  
273 antibodies have already been tested in human subjects, and been found to have therapeutic activity,  
274 including antibody VRC01 (23, 64, 65). To determine whether BG24 shows therapeutic potential  
275 *in vivo*, we sought to compare its anti-HIV activity with well-established antibody VRC01 in  
276 HIV<sub>YU2</sub>-infected humanized mice. While the pharmacokinetics of VRC01 are known, we first  
277 evaluated the pharmacokinetic properties of BG24 by intravenous injection into non-humanized  
278 NOD-Rag1<sup>null</sup> IL2r<sup>g</sup><sup>null</sup> (NRG) mice (n=6). BG24 showed a similar decline in serum to other  
279 VRC01-class antibodies indicating an acceptable pharmacokinetic profile (Fig. S7) (34).

280 We then infected humanized NRG mice intraperitoneally with HIV<sub>YU-2</sub> and subsequently  
281 treated them subcutaneously with repeated monotherapy of antibody BG24 (n=6), antibody  
282 VRC01 (n=6), or left them untreated (n=6) (Fig. 5A). While untreated mice showed stable viremia  
283 over the course of 4 weeks, mice treated with BG24 or VRC01 showed a comparable peak drop in  
284 average viral load of 0.54 and 0.57 log<sub>10</sub> copies/ml, respectively (Fig. 5A). In both treatment  
285 groups, rebound of viremia occurred by 3 weeks post treatment initiation. To study viral escape  
286 mutations from BG24 *in vivo*, we performed single genome sequencing of HIV-1 envelope from

287 mouse plasma of three BG24-treated mice at four weeks after therapy initiation (Fig. 5B). All 22  
288 sequences obtained harbored one or more recurrent mutations in the D-loop, CD4-binding loop or  
289 V5-loop region, including well-known mutations N279K, N280D and G459D which have been  
290 associated with CD4-binding site antibody escape (18, 34, 66). 18 post-rebound sequences were  
291 obtained from three mice treated with VRC01 which showed a similar escape mutation profile  
292 with recurrent mutations also including N279K, N280D and G459D (Fig. 5B). Neutralization  
293 testing of BG24 and VRC01 on an extended HIV<sub>YU2</sub> site mutant panel further confirmed their  
294 similar mutational sensitivity profile (Table S6). We conclude that BG24 has similar therapeutic  
295 efficacy to VRC01 in HIV<sub>YU2</sub>-infected humanized mice, highlighting that BG24-like antibodies  
296 retain activity *in vivo*.

297

### 298 **Single genome sequencing of 391370's plasma Env**

299 In order to better understand the viral context in which BG24 arose, and to investigate selective  
300 pressure exerted by BG24 on Env, we sequenced contemporaneous plasma envelope of subject  
301 391370 using single genome sequencing. We obtained 24 intact full-length Env sequences, which  
302 all mapped conclusively as Clade B. As has been described in other elite neutralizers such as  
303 CH505 (5, 67), a high-level of diversity was evident in the Env quasispecies of 391370. The Env  
304 phylogeny segregated into two major branches that exhibited an average sequence difference of  
305 more than 20% of Env nucleotides (Fig. S8). Consistent with selective pressure being exerted by  
306 the BG24 family, we observed positive selection for known CD4-binding site escape mutations in  
307 the D-loop (D279K, D279R, A281T), and the b23-V5 loop region (G459D, addition of a glycan  
308 in V5), and all sequences carried a PNGS at 276<sub>gp120</sub> (Fig. 5C).

309

## 310 **The role of somatic hypermutation in enhancing potency and breadth**

311 Analysis of the BG24 paratope revealed 50% of the paratope surface to involve V-gene regions of  
312 both heavy and light chains, and an additional 22% attributed to CDR3 regions (Fig. 6A,B). Thus,  
313 only 28% of paratope residues were altered by somatic hypermutation, with the majority of somatic  
314 hypermutations occurring in CDR loops. Somatic mutations in FWR1 and CDRH1 mediated  
315 interprotomer gp120 contacts, while mutations in CDRL1 (including a 6 amino acid deletion) were  
316 necessary for accommodating the N276<sub>gp120</sub>-glycan at the CD4bs, consistent with other VRC01-  
317 class bNAbs (Fig. 6C-E). Interestingly, BG24 somatic hypermutation primarily modified CDRH2  
318 and neighboring FWR sequence motifs to provide potential H-bonding to the CD4bs loop (Fig.  
319 6F).

320 To better define somatic hypermutations in BG24, we designed several heavy and light  
321 chain constructs to determine regions that played an essential role in its neutralization breadth and  
322 potency. Inclusion of the 6-residue CDRL1 deletion in the BG24 LC did not result in any  
323 appreciable binding or neutralization to Env isolates containing the N276<sub>gp120</sub>-glycan with the  
324 exception of the clade D isolate, 6405. Thus, all minimal constructs were constructed to maintain  
325 the N276<sub>gp120</sub>-glycan accommodating CDRL1 deletion (Fig. 6A), similar to the previously  
326 described MinVRC01 (37). Reversion of somatic hypermutations in the FWRs, CDRH1, and  
327 CDRL2, yielded a minimally-mutated BG24 construct that showed ~85% neutralization breadth  
328 on the global 12-strain viral panel with a geometric mean IC<sub>50</sub> of 1.56 µg/mL (Fig. 6A,G). This  
329 observation is consistent with longitudinal analysis of PCIN63 maturation where early  
330 convergence of CDRH2 motifs was critical to heterologous activity (38).

331

## 332 **Discussion**

333 VRC01-class bNAbs have long been a target for rational vaccine design given their near pan-  
334 neutralizing activity across HIV-1 viral clades (32, 68). However, despite success in the isolation  
335 of numerous VRC01-class bNAbs, the prospect of eliciting such antibodies in vaccination efforts  
336 has been hampered by the high mutational count of these antibodies (32, 61, 68). Recent B-cell  
337 repertoire data suggests that the frequency of SHM observed in archetypal VRC01-class bNAbs  
338 ranks far above the average SHM frequency in the B-cell repertoires of HIV-naïve individuals  
339 (69). Indeed, it was suggested that such heavily mutated bNAbs might only arise in the context of  
340 HIV-1 infection and associated changes in normal B-cell selection processes. Easier blueprints for  
341 potent and broad CD4bs antibodies that might be more readily elicited by vaccination, therefore,  
342 remain an area of strong interest. Here, we studied the antibody response of a viremic controller  
343 and identified VRC01-class antibody BG24 that might represent one such easier blueprint for  
344 CD4-binding site based HIV vaccine design.

345

346 Our results indicate that there are exceptions to the commonly-held rule that high levels of somatic  
347 hypermutation are a pre-requisite for the breadth and potency of VRC01-class antibodies (70, 71).  
348 While it had been previously demonstrated that minimally mutated VRC01-class antibodies can  
349 be constructed through *in-silico* based design (37), only one naturally arising VRC01-class  
350 antibody lineage, the PCIN63 family, with a shorter maturation path and comparable neutralization  
351 activity to VRC01 has been described to date (38). Similarly, to the PCIN63 lineage, antibody  
352 BG24 shows low rates of SHM in a range of <15% on nucleotide level in both heavy and light  
353 chain, a range of mutation that might be more readily achievable by vaccination. Indeed, we found  
354 that only 28% of the BG24 paratope was modified by SHM and found key mutations to be focused  
355 within specific regions, in particular CDRH2 and heavy chain framework residues. In line with

356 these findings and previous data (56), we were able to show that it is possible to construct even  
357 less mutated versions of BG24-type antibodies that exhibit high breadth and modest neutralization  
358 with <10% SHM on the amino acid level.

359

360 Taken together, BG24 and the PCIN63 lineage indicate that multiple shorter mutational pathways  
361 to VRC01-class type recognition of the CD4-binding site exist. Indeed, the two bNAbs arose in  
362 the context of different infecting viral clades, as PCIN63 arose in a Clade C infected donor, while  
363 BG24 arose in a Clade B infected donor. Moreover, while PCIN63 utilizes an IGK1-5\*03 light  
364 chain and accommodates the N276<sub>gp120</sub>-glycan through CRDL1 flexibility, BG24 employs an  
365 IGLV2-11\*01 light chain and accommodates the N276<sub>gp120</sub>-glycan through a 6 amino-acid CRDL1  
366 deletion. In contrast to some other VRC01-class antibodies, neither of the two antibodies carries  
367 insertions or deletions in the heavy chain. Overall, the heavy chain sequences of these two  
368 antibodies are quite divergent with 29.2% difference on amino acid level in their V-gene portions  
369 despite both appearing to be derived from IGHV1-2\*02 germline genes, suggesting that the  
370 trajectory of VRC01-class bNAb affinity maturation is not limited and can sample diverse  
371 sequences at key contact residues.

372

373 Providing support for the notion that such VRC01-class antibodies with short maturational  
374 pathways retain stability and potential for anti-HIV activity *in vivo*, we were able to demonstrate  
375 that BG24 had comparable therapeutic *in vivo* efficacy to VRC01 in humanized mice. We also did  
376 not find any indication of auto- or polyreactivity of BG24 suggesting that such phenomena might  
377 not be an impediment to BG24-type antibody induction. Moreover, engineered constructs that  
378 encoded neutralizing enhancing mutations in CDRH2, including the G54WHC mutation, also

379 showed no polyreactivity, suggesting that improvement of such antibodies for therapeutic use can  
380 be achieved.

381

382 Structural studies of BG24 bound to a BG505 and DU422 Env trimers demonstrated that BG24  
383 exhibited a conserved binding orientation relative to more mutated VRC01-class bNAbs,  
384 maintaining critical germline and CDR3 interactions, but established interprotomer contacts with  
385 the adjacent gp120. While the overall binding orientation of BG24 to Env was conserved, BG24  
386 deviates from other VRC01-class antibodies in signature sequence features, including in particular  
387 the use of a Tyr instead of a Trp in the -5 position of the CDRH3 and also does not exhibit the  
388 consensus QQYEF CRDL3 motif of the VRC01-class antibodies that are derived from kappa  
389 germline genes. Indeed, BG24 belongs to the less frequently described group of VRC01-class  
390 antibodies that use a lambda light chain and is the second IGLV2-11\*01 CD4bs bNAb lineage  
391 isolated to date (51, 57).

392

393 A recent study that assessed binding of B-cell receptors in the immune repertoire of HIV-naïve  
394 individuals to the CD4bs immunogen eOD-GT8 identified lambda light chain-using VRC01-class  
395 antibody precursors with a Tyr residue at the -5 position of CDRH3 (54), supporting the notion  
396 that BG24 precursors exist widely. In contrast to the previously dominating assumption that a Trp  
397 in CDRH3 position -5 is key, BG24's properties actually demonstrate that a Tyr at the -5 position  
398 can even be favorable in specific instances, as we found that replacement of Tyr with a Trp reduced  
399 neutralization activity. This suggests that these naïve B-cells isolated from HIV-uninfected donors  
400 using eOD-GT8 or other VRC01-class germline-targeting immunogens may represent bona-fide  
401 VRC01-class bNAb precursors with potential to develop into BG24-type CD4-binding site bNAbs.

402

403 Collectively, our data suggests that BG24-type antibodies represent a potential target for CD4-  
404 binding site directed HIV vaccine design. Future studies will be required to explore whether  
405 boosting immunogens will be able to shepherd presumed BG24 B-cell precursors to reach broad  
406 and potent neutralization, in particular given that the N276<sub>gp120</sub>-glycan barrier still presents a major  
407 hurdle towards these efforts. Overall, the discovery of donor-derived minimally-mutated VRC01-  
408 class bNAbs and their intermediates raises the possibility that immunization schemes that might  
409 drive such responses are within reach.

## 410 **Materials and Methods:**

### 411 **Patient samples**

412 Subject 391370 was a participant in The Ragon Institute of MGH, MIT and Harvard protocol ‘Host  
413 Genetics, Immunology and Virology of HIV’ from October 2005 to April 2008. The protocol was  
414 approved by the MGH IRB (2003P001678/MGH). Biological samples were obtained and analyzed  
415 under protocol MNU-0625 approved by the Rockefeller IRB. The subject is an African American  
416 male originally diagnosed with HIV-1 in 1990 who was always ART-naïve until the end of the  
417 study follow-up. B-cell sorting was done on two aliquots of a peripheral blood mononuclear cell  
418 (PBMC) sample from 2007. During the period of observation, viral loads ranged from 215 to  
419 27,400 copies/ml (geometric mean: 795 copies/ml) and CD4<sup>+</sup> T-cell counts from 352-495 cells/ $\mu$ l  
420 (mean: 413 cells/ $\mu$ l). Polyclonal IgG from subject 391370 was isolated from heat-inactivated  
421 plasma using Protein G Sepharose 4 Fast Flow (GE Healthcare). Purified IgG was buffer  
422 exchanged into Dulbecco’s Phosphate Buffered Saline (DPBS) and sterile-filtered prior to  
423 neutralization testing.

424

### 425 **Neutralization testing by TZM.bl and neutralization fingerprinting**

426 A luciferase-based TZM.bl assay was used to measure the neutralizing activity of polyclonal IgG  
427 and monoclonal antibodies according to standard protocols (72). Each assay was performed at least  
428 in duplicates. To determine 50% (IC<sub>50</sub>) or 80% (IC<sub>80</sub>) inhibitory concentrations, 5-parameter curve  
429 fitting was utilized. Non-specific activity was detected by testing against murine leukemia virus  
430 (MuLV). Analysis of neutralization and graphing was done using the Antibody Database (v 2.0)  
431 (73). In order to determine the neutralization fingerprint of the polyclonal IgG/monoclonal  
432 antibodies, a panel of 20 HIV-1 strains (f61 panel) was used as described (42, 74).

433

#### 434 **Single B-cell bait-sorting**

435 Single B-cell sorting of IgG<sup>+</sup> memory B-cells was done using BG505.SOSIP.664 as bait in a  
436 manner previously described with slight modifications (44, 75, 76). Avi-tagged  
437 BG505.SOSIP.664 (BG505.SOSIP.664.Avi) was produced in CHO cells and purified using a  
438 PGT145 affinity column as described (76, 77). BG505.SOSIP.664.Avi was biotinylated using the  
439 BirA-Ligase (Avidity) following the manufacturer's instructions, and an aliquot of 5 µg of  
440 biotinylated BG505.SOSIP.664 was then freshly coupled to Streptavidin-PE in a volume of 10 µl  
441 DPBS immediately before sorting. Two independent sorts on 10 million PBMCs each were carried  
442 out. In the first sort, fluorescent staining of total PBMCs was done using CD3-PerCP-Cy5.5, CD14  
443 PerCP-Cy5.5, CD335 PerCP-Cy5.5, CD606 PerCP-Cy5.5, CD19 BV421, CD20 BV421, IgG  
444 BV510, IgM BV605 and fluorescently-labelled BG505 bait. The staining for the second sort  
445 included the same antibodies with the addition of LIVE/DEAD Fixable Aqua. Stainings were  
446 performed for 30 mins at 4 °C, and cell sorting was done on a FACS Aria II. BG505-binding IgG<sup>+</sup>  
447 memory B-cells were sorted directly into lysis buffer in 96-well plates (78, 79). Amplification of  
448 B-cell heavy and light chain variable regions was done as described (41, 44), and bands from  
449 positive wells were subjected to Sanger Sequencing. Analysis of obtained antibody gene sequences  
450 was done using IgBLAST and the international ImMunoGeneTics information system (IMGT).  
451 For recombinant production, antibody variable regions were cloned into human Igγ1-, Igκ or Igλ-  
452 expression vectors by sequence and ligation independent cloning (SLIC). Recombinant expression  
453 of antibodies was done using transient transfection of 293-6E cells followed by Protein G  
454 purification. Antibodies for neutralization, and *in vivo* studies were buffer exchanged into DPBS  
455 using Amicon Ultra centrifugal filters.

456

### 457 **Phylogenetic analysis of BG24 clonal members**

458 The human IgV<sub>H</sub>1-2\*02 allele sequence was sourced from the international ImMunoGeneTics  
459 information system (IMGT) (80). Heavy chain nucleotide sequences of the BG24 clonal family  
460 were aligned with the IgV<sub>H</sub>1-2\*02 germline sequence in Geneious R8 (v8.1.9) using MUSCLE.  
461 The maximum-likelihood tree was then generated with the RAxML plugin (v 7.2.8) using a GTR  
462 Gamma model and the ‘Rapid Bootstrapping and search for best-scoring ML tree’ function with  
463 100 bootstrap replicates. Formatting of the best-scoring ML tree was done using FigTree (v1.4.3).

464

### 465 **Autoreactivity and polyreactivity assays**

466 Autoreactivity of antibody BG24 and the two reference antibodies 4E10 and 2F5 was evaluated  
467 with the commercially-available HEp-2 based assay NOVA Lite kit (Inova Diagnostics). Testing  
468 was performed at an IgG concentration of 25 µg/ml. Photographing of slides was done on a Leica  
469 DMI 6000 B with 800 ms exposure, Gain of 10 and an intensity of 100%. Measurements were  
470 performed in duplicate.

471

472 Baculovirus-based polyreactivity assays were conducted using ELISA detection of non-specific  
473 binding as described (63). Briefly, a solution of 1% baculovirus particles in 100mM sodium  
474 bicarbonate buffer pH 9.6 was absorbed onto the wells of a 384-well ELISA plate (Nunc Maxisorp)  
475 using a Tecan Freedom Evo liquid handling robot. The plate was incubated overnight at 4°C  
476 followed by a 1 h block at room temperature with PBS + 0.5% BSA. Purified IgGs (diluted to 1  
477 µg/mL in PBS + 0.5% BSA) were added to the blocked assay plate and incubated for 3 hours at  
478 room temperature. Bound IgG was detected as the luminescence signal at 425 nm using an HRP-

479 conjugated anti-human IgG (H&L) secondary antibody (Genscript) and SuperSignal ELISA Femto  
480 Maximum Sensitivity Substrate (Thermo Fisher Scientific).

481

## 482 ***In vivo* experiments**

483 Mouse experiments were approved by the State Agency for Nature, Environment and Consumer  
484 Protection (LANUV) of North-Rhine Westphalia. NOD-Rag1<sup>null</sup> IL2rg<sup>null</sup> (NRG) mice were  
485 purchased from The Jackson Laboratory. NRG mice were bred and maintained at the Dezentrales  
486 Tierhaltungsnetzwerk Weyertal at University of Cologne. Assessment of the pharmacokinetics of  
487 BG24 was done in non-humanized NRG mice. Mice were injected intravenously with 250 µg of  
488 BG24 (n=6) via the tail vein. Facial vein bleedings were done on days 1,3,6,9 and 14 post injection,  
489 and serum levels of the antibodies were measured using a total IgG ELISA as previously described  
490 (18). To generate humanized mice for HIV-1 treatment experiments, an established protocol was  
491 followed with slight modifications (18, 81). In brief, sub-lethally irradiated 1-5 day old NRG mice  
492 were injected intra-hepatically with CD34<sup>+</sup> hematopoietic stem cells (HSCs) and screened for  
493 humanization by flow cytometry 12-weeks post HSC injection. HSCs were purified from cord  
494 blood or perfused human placental tissues using magnetic bead based purification (Miltenyi). The  
495 stem cell isolation protocol was approved by the ethics committee of the Medical Faculty of the  
496 University of Cologne. All stem cell donors provided written informed consent.

497

498 For antibody treatment experiments, HIV-1 infection of humanized mice was performed  
499 intraperitoneally using HIV-1<sub>YU2</sub> (82, 83). For viral load measurements, mice were bled from the  
500 facial vein into EDTA tubes (Sarstedt). Viral RNA was subsequently isolated from mouse plasma  
501 using the MinElute Virus Kit (Qiagen) on the QiaCube. Measurements of HIV-1 levels in plasma  
502 were done using an in-house quantitative PCR assay that amplifies a part of pol (82) using the

503 TaqMan® RNA-to-Ct™ 1-Step Kit on a Roche LightCycler 480 Instrument II. The primers used  
504 in the qPCR were: 5'-TAATGGCAGCAATTTACCA- 3' and 5'-  
505 GAATGCCAAATTCCTGCTTGA-3', the probe was 5'-/56-  
506 FAM/CCCACCAAC/ZEN/ARGCRGCCTTAACTG/3IABkFQ/-3'. The assay was determined to  
507 have a limit of accuracy of 384 copies/ml (based on the standard curve used). Before starting  
508 treatment, viral loads of mice were measured two times. Only mice with viral loads of more than  
509 4,000 copies/ml prior to treatment were used in experiments. Antibody injections were done  
510 subcutaneously. Treatment was initiated with a loading dose of 1 mg of each antibody, and mice  
511 subsequently received 0.5 mg of each antibody every 3 days for a total of 3 weeks.

512

### 513 **Single genome sequencing of mouse plasma HIV-1 env genes**

514 Single genome sequencing of mouse plasma env genes was carried out as described previously  
515 (44). In brief, complementary DNA (cDNA) was generated from extracted mouse plasma RNA  
516 using primer YB383 5'-TTTTTTTTTTTTTTTTTTTTTTTTTTTTRAAGCAC-3' and enzyme  
517 Superscript III (Invitrogen) according to manufacturer's instructions. Synthesized cDNA was  
518 subsequently serially diluted and subjected to two rounds of nested PCR using Platinum Taq Green  
519 Hot Start (Thermo Fisher Scientific) and primers specifically adapted for amplification of env of  
520 HIV<sub>YU2NL4-3</sub> (1<sup>st</sup> round primers: YB383 and YB50 5'-  
521 GGCTTAGGCATCTCCTATGGCAGGAAGAA-3'; 2<sup>nd</sup> round primers YB49 5'-  
522 TAGAAAGAGCAGAAGACAGTGGCAATGA-3', YB52 5'-  
523 GGTGTGTAGTTCTGCCAATCAGGGAAGWAGCCTTGTG-3'). Bands of proper size from  
524 amplifications with less than 30% efficiency were PCR-purified using the Nucleospin Gel and  
525 PCR-Clean Up kit (Macherey Nagel, 740609.250) and then Sanger sequenced. Assembly of Env

526 sequences was done using the Geneious 8.1.9 (Biomatters) de-novo assembly tool. Sequences with  
527 full coverage of gp160 Env were used in downstream analyses.

528

### 529 **Single genome sequencing of patient HIV-1 Env genes**

530 Single HIV-1 genomes encoding HIV-1 gp160 were amplified from patient plasma according to a  
531 previously published protocol (84-86). In brief, viral RNA was isolated from patient plasma using  
532 the Virus Mini Spin Kit on a QiaCube. Isolated viral RNA was then used to generate  
533 complementary DNA (cDNA) using Superscript III according to manufacturer's instructions with  
534 the primer envB3out (5'- TTGCTACTTGTGATTGCTCCATGT-3'). The HIV-1 env gene was  
535 then amplified through a nested PCR approach using Platinum Taq. 1<sup>st</sup> round primers were:  
536 envB5out 5'-TAGAGCCCTGGAAGCATCCAGGAAG-3' and envB3out 5'-  
537 TTGCTACTTGTGATTGCTCCATGT-3'; 2<sup>nd</sup> round primers were: envB5in 5' -  
538 TTAGGCATCTCCTATGGCAGGAAGAAG-3' and envB3in 5'-  
539 GTCTCGAGATACTGCTCCCACCC-3'. PCRs were carried out using serial dilutions of cDNA  
540 to obtain a range in which less than 30% of wells generated a band. Positive wells from  
541 amplifications that yielded less than 30% of bands were subjected to library preparation with the  
542 Nextera DNA Amplification Kit. Env libraries were sequenced on an Illumina MiSeq (2x 150 bp  
543 Nano Kit) and assembled to the best HIV-1 Env reference sequence from HIV Blast using an in-  
544 house pipeline (84). Only intact Env sequences with a maximum of one ambiguity were used in  
545 downstream analyses. To generate the maximum-likelihood tree of subject 391370's plasma env  
546 sequences, env nucleotide sequences were aligned in Geneious R8 (v8.1.9) using ClustalW. The  
547 maximum-likelihood tree was then generated with the RAxML plugin (v 7.2.8) using a GTR

548 Gamma model and the ‘Rapid Bootstrapping and search for best-scoring ML tree’ function with  
549 100 bootstrap replicates. The best-scoring ML tree was formatted using FigTree (v1.4.3).

550

551

## 552 **Protein expression and purification for structural studies**

553 Fabs and IgGs used in this study were produced as described (44). Briefly, Fabs and IgGs were  
554 expressed by transiently transfecting Expi293 cells with vectors encoding the appropriate heavy  
555 and light chain genes. Secreted Fabs or IgGs were purified from cell supernatants using Ni<sup>2+</sup>-NTA  
556 (Fabs) or Protein A affinity chromatography (IgGs) followed by size exclusion chromatography  
557 (SEC) with a Superdex200 16/60 column (Cytiva). Purified proteins were concentrated and  
558 maintained at 4 °C in storage buffer (20 mM Tris pH 8.0, 150 mM NaCl, 0.02% sodium azide).

559

560 Genes encoding soluble BG505 SOSIP.664 or DU422 SOSIP.664 gp140 trimers were stably  
561 expressed in Chinese hamster ovary cells as described (77, 87). Secreted Env trimers expressed in  
562 the absence of glycosylation inhibitors were isolated from cell supernatants using PGT145  
563 immunoaffinity chromatography by covalently coupling PGT145 IgG monomer to an activated-  
564 NHS Sepharose column (Cytiva) as described (88). Trimers were eluted using 3M MgCl<sub>2</sub>,  
565 dialyzed into storage buffer, and purified using a Superdex200 16/60 column (Cytiva) against the  
566 same buffer. Peak fractions pertaining to SOSIP trimers were pooled and repurified using the same  
567 column and buffer conditions. Individual fractions were stored separately at 4 °C.

568

## 569 **Crystal structures of BG24<sub>S60A</sub> Fab and a BG24<sub>S60A</sub>-BG505-10-1074 complex**

570 A complex of BG24<sub>S60A</sub>-BG505-101074 was assembled by incubating purified BG24<sub>S60A</sub> Fab with  
571 BG505 SOSIP.664 trimer at a 3:1 Fab:gp120-protomer molar ratio. Following overnight  
572 incubation at RT, 10-1074 Fab was incubated with the complex at a 3:1 Fab:gp120-protomer molar  
573 ratio for 5 h, and complexes were purified from unbound Fab by SEC on a Superose 6 10/300  
574 column (Cytiva) run in 20 mM Tris pH 8 and 100 mM NaCl. Purified complexes were concentrated  
575 to 5-10 mg/mL by centrifugation with a 100 kDa concentrator (Millipore). Unliganded BG24<sub>S60A</sub>  
576 Fab was concentrated to 10-15 mg/mL by centrifugation with a 30-kDa concentrator (Millipore).

577

578 Initial matrix crystallization trials against 576 conditions were performed at room temperature  
579 using the sitting drop vapor diffusion method by mixing equal volumes of protein sample and  
580 reservoir using a TTP LabTech Mosquito robot and commercially-available screens (Hampton  
581 Research and Qiagen). Initial hits were optimized and crystals for unliganded BG24<sub>S60A</sub> were  
582 obtained in 0.25 M potassium chloride, 18% polyethylene glycol (PEG) 3350 at 20 °C. Crystals  
583 for the BG24<sub>S60A</sub>-BG505-101074 complex were obtained in 0.1 M Bis-Tris pH 6.5, 20%  
584 PEG1500. Crystals were cryo-protected stepwise to 20% glycerol before being cryopreserved in  
585 liquid nitrogen.

586

587 X-ray diffraction data were collected for both samples at the Stanford Synchrotron Radiation  
588 Lightsource (SSRL) beamline 12-2 on a Pilatus 6M pixel detector (Dectris). Data from a single  
589 crystal were indexed and integrated in XDS (89) and merged with AIMLESS in the *CCP4* software  
590 suite (90). The unliganded BG24<sub>S60A</sub> structure was determined by molecular replacement in  
591 PHASER (91) using a single search with coordinates of the VRC-PG20 Fab (PDB 4LSU) after  
592 removal of CDR loops. Coordinates from a refined BG24<sub>S60A</sub> model were used in combination

593 with a gp140-10-1074 complex (PDB 5T3Z) as search models for the BG24<sub>S60A</sub>-BG505-101074  
594 complex data. Models generated by molecular replacement were refined using B-factor refinement  
595 in Phenix (92), followed by several cycles of manual building with B factor sharpening in Coot  
596 (93). For the 2.0Å BG24<sub>S60A</sub> Fab structure, TLS refinement was also performed.

597

### 598 **Cryo-EM sample preparation**

599 A complex of BG24<sub>CDR2-v2</sub>-DU422-101074 was assembled by incubating purified BG24<sub>CDR2-v2</sub>  
600 Fab with DU422 SOSIP.664 trimer at a 1.2:1 Fab:gp120-protomer molar ratio. Following  
601 overnight incubation at RT, 10-1074 Fab was incubated with the complex at a 1.2:1 Fab:gp120-  
602 protomer molar ratio for 5 h. BG24<sub>CDR2-v2</sub>-DU422-101074 complexes were concentrated to 1-2  
603 mg/ml in 20 mM Tris pH 8 and 100 mM NaCl, and 3 µl was added to Quantifoil R1.2/1.3 300  
604 mesh copper grid (Electron Microscopy Services) that had been freshly glow-discharged using a  
605 PELCO easiGlow (Ted Pella). Samples were immediately vitrified in 100% liquid ethane using a  
606 Mark IV Virtoblot (ThermoFisher) by blotting for 3-4s with Whatman No. 1 filter paper at 20°C  
607 and 100% relative humidity.

608

### 609 **Cryo-EM data collection and processing**

610 Single-particle cryo-EM data were collected on a Talos Arctica transmission electron microscope  
611 (ThermoFisher) operating at 200 kV, using a 3x3 beam image shift pattern with SerialEM  
612 automated data collection software (94). Movies were collected on a Gatan K3 Summit direct  
613 electron detector (DED) operating in counting mode at a nominal magnification of 45,000x (super-  
614 resolution 0.4345 Å/pixel) using a defocus range of -1.0 µm to -2.5 µm. Movies were collected

615 with an 3.6 s exposure time with a rate of 13.5 e<sup>-</sup>/pix/s, which resulted in a total dose of ~60 e<sup>-</sup>/Å<sup>2</sup>  
616 over 40 frames.

617

618 Data processing was conducted as previously described (44). Briefly, movies were motion  
619 corrected and doseweighted using MotionCor2 in RELION-3 (95). Non-dose weighted summed  
620 images were used for CTF determination using Gctf (96), and reference-free particle picking was  
621 achieved using Laplacian-of-Gaussian filtering in RELION-3 (95). An initial stack of 455,671  
622 particles were extracted from 1,180 dose-weighted micrographs and subjected to reference-free  
623 2D classification. A total of 310,246 particles corresponding to class averages that displayed  
624 secondary-structural elements and represented views different views of Fab bound Env-trimer  
625 were extracted and re-centered prior to heterogenous ab initio model generation using cryoSPARC  
626 v2.2 (97).

627

628 The generated volume was low-passed filtered to 60 Å and used as an initial model for 3D auto-  
629 refinement in RELION-3 (C1 symmetry, k=8). After 25 iterations, a soft mask was generated from  
630 the highest-resolution model (5-pixel extension, 10-pixel soft cosine edge), and used in an  
631 additional round of 3D classification. This procedure yielded a particle stack of 248,600 particles  
632 that was homogeneously refined in Relion using a soft mask in which Fab constant domains were  
633 masked out. 3D classification was repeated without alignments and 204,220 particles were  
634 subjected to particle polishing, CTF refinement, and subsequent rounds of homogenous refinement  
635 with C3 symmetry applied. Refinement procedures produced a final estimated global resolution of  
636 3.5Å Å according to gold-standard FSC (98).

637

638 **Modeling and refinement of cryo-EM structures**

639 For the final reconstruction of BG24<sub>CDR2-v2</sub>-DU422-10-1074, initial coordinates were generated by  
640 docking a refined BG24<sub>S60A</sub>-BG505-10-1074 reference model (this work) into the cryo-EM  
641 density using UCSF Chimera v1.13 (99). After sequence matching to DU422 gp140, initial models  
642 were refined into the EM maps using one round of rigid body, morphing, and simulated annealing  
643 followed by subsequent rounds of B-factor refinement in Phenix (92). Models were manually built  
644 following iterative rounds of real-space and B-factor refinement in Coot (93) and Phenix (92) with  
645 secondary structure restraints. Modeling of glycans was achieved by interpreting cryo-EM density  
646 at PNGS in Coot using a map with a  $-150 \text{ \AA}^2$  B-factor sharpening value, contoured at  $3\sigma$  due to  
647 the lower resolution of glycans at the periphery of the structure. Validation of model coordinates  
648 was performed using MolProbity (100) and Privateer (101).

649

650 **Structural and bioinformatic analyses**

651 Superpositions and figures were rendered using PyMOL (Version 1.5.0.4 Schrodinger, LLC), and  
652 protein electrostatic calculations were done using APBS and PDB2PQR webservers (102). Buried  
653 surface areas (BSAs) were determined with PDBePISA using a  $1.4 \text{ \AA}$  probe (103). Potential  
654 hydrogen bonds were assigned using a distance of  $<3.6 \text{ \AA}$  and an A-D-H angle of  $>90^\circ$ , while the  
655 maximum distance allowed for a van der Waals interaction was  $4.0 \text{ \AA}$ . Putative H-bonds, van der  
656 Waals assignments and total BSA should be considered tentative, owing to the relatively low  
657 structure resolutions. Computational analysis of neutralization panel data (Table S7) was done as  
658 previously described (73).

659

660

661 **References:**

- 662 1. Z. Euler *et al.*, Activity of broadly neutralizing antibodies, including PG9, PG16, and  
663 VRC01, against recently transmitted subtype B HIV-1 variants from early and late in the  
664 epidemic. *J Virol* **85**, 7236-7245 (2011).
- 665 2. E. Falkowska *et al.*, Broadly neutralizing HIV antibodies define a glycan-dependent  
666 epitope on the prefusion conformation of gp41 on cleaved envelope trimers. *Immunity* **40**,  
667 657-668 (2014).
- 668 3. A. J. Hessel *et al.*, Broadly neutralizing human anti-HIV antibody 2G12 is effective in  
669 protection against mucosal SHIV challenge even at low serum neutralizing titers. *PLoS*  
670 *Pathog* **5**, e1000433 (2009).
- 671 4. A. J. Hessel *et al.*, Broadly neutralizing monoclonal antibodies 2F5 and 4E10 directed  
672 against the human immunodeficiency virus type 1 gp41 membrane-proximal external  
673 region protect against mucosal challenge by simian-human immunodeficiency virus  
674 SHIVBa-L. *Journal of virology* **84**, 1302-1313 (2010).
- 675 5. H. X. Liao *et al.*, Co-evolution of a broadly neutralizing HIV-1 antibody and founder  
676 virus. *Nature* **496**, 469-476 (2013).
- 677 6. M. Malbec *et al.*, Broadly neutralizing antibodies that inhibit HIV-1 cell to cell  
678 transmission. *J Exp Med* **210**, 2813-2821 (2013).
- 679 7. L. E. McCoy, D. R. Burton, Identification and specificity of broadly neutralizing  
680 antibodies against HIV. *Immunol Rev* **275**, 11-20 (2017).
- 681 8. H. Mouquet *et al.*, Complex-type N-glycan recognition by potent broadly neutralizing  
682 HIV antibodies. *Proceedings of the National Academy of Sciences of the United States of*  
683 *America* **109**, E3268-3277 (2012).
- 684 9. J. F. Scheid *et al.*, Broad diversity of neutralizing antibodies isolated from memory B  
685 cells in HIV-infected individuals. *Nature* **458**, 636-640 (2009).
- 686 10. J. F. Scheid *et al.*, Sequence and structural convergence of broad and potent HIV  
687 antibodies that mimic CD4 binding. *Science* **333**, 1633-1637 (2011).
- 688 11. C. O. Barnes *et al.*, Structural characterization of a highly-potent V3-glycan broadly  
689 neutralizing antibody bound to natively-glycosylated HIV-1 envelope. *Nat Commun* **9**,  
690 1251 (2018).
- 691 12. H. B. Gristick *et al.*, Natively glycosylated HIV-1 Env structure reveals new mode for  
692 antibody recognition of the CD4-binding site. *Nature structural & molecular biology* **23**,  
693 906-915 (2016).
- 694 13. J. S. McLellan *et al.*, Structure of HIV-1 gp120 V1/V2 domain with broadly neutralizing  
695 antibody PG9. *Nature* **480**, 336-343 (2011).
- 696 14. M. Pancera *et al.*, Structure and immune recognition of trimeric pre-fusion HIV-1 Env.  
697 *Nature* **514**, 455-461 (2014).
- 698 15. A. B. Ward, I. A. Wilson, The HIV-1 envelope glycoprotein structure: nailing down a  
699 moving target. *Immunol Rev* **275**, 21-32 (2017).
- 700 16. C. K. Wibmer, P. L. Moore, L. Morris, HIV broadly neutralizing antibody targets. *Curr*  
701 *Opin HIV AIDS* **10**, 135-143 (2015).
- 702 17. N. L. Haigwood *et al.*, Passive immunotherapy in simian immunodeficiency virus-  
703 infected macaques accelerates the development of neutralizing antibodies. *J Virol* **78**,  
704 5983-5995 (2004).

- 705 18. F. Klein *et al.*, HIV therapy by a combination of broadly neutralizing antibodies in  
706 humanized mice. *Nature* **492**, 118-122 (2012).
- 707 19. P. W. Parren *et al.*, Antibody protects macaques against vaginal challenge with a  
708 pathogenic R5 simian/human immunodeficiency virus at serum levels giving complete  
709 neutralization in vitro. *Journal of virology* **75**, 8340-8347 (2001).
- 710 20. M. Shingai *et al.*, Passive transfer of modest titers of potent and broadly neutralizing anti-  
711 HIV monoclonal antibodies block SHIV infection in macaques. *The Journal of*  
712 *experimental medicine* **211**, 2061-2074 (2014).
- 713 21. M. Caskey *et al.*, Viraemia suppressed in HIV-1-infected humans by broadly neutralizing  
714 antibody 3BNC117. *Nature* **522**, 487-491 (2015).
- 715 22. P. Mendoza *et al.*, Combination therapy with anti-HIV-1 antibodies maintains viral  
716 suppression. *Nature* **561**, 479-484 (2018).
- 717 23. R. M. Lynch *et al.*, Virologic effects of broadly neutralizing antibody VRC01  
718 administration during chronic HIV-1 infection. *Science translational medicine* **7**,  
719 319ra206 (2015).
- 720 24. K. E. Stephenson *et al.*, Safety, pharmacokinetics and antiviral activity of PGT121, a  
721 broadly neutralizing monoclonal antibody against HIV-1: a randomized, placebo-  
722 controlled, phase 1 clinical trial. *Nat Med* **27**, 1718-1724 (2021).
- 723 25. D. R. Burton, L. Hangartner, Broadly Neutralizing Antibodies to HIV and Their Role in  
724 Vaccine Design. *Annu Rev Immunol* **34**, 635-659 (2016).
- 725 26. A. Escolano, P. Dosenovic, M. C. Nussenzweig, Progress toward active or passive HIV-1  
726 vaccination. *The Journal of experimental medicine* **214**, 3-16 (2017).
- 727 27. A. Escolano *et al.*, Sequential immunization of macaques elicits heterologous  
728 neutralizing antibodies targeting the V3-glycan patch of HIV-1 Env. *Science*  
729 *translational medicine* **13**, eabk1533 (2021).
- 730 28. R. Kong *et al.*, Antibody Lineages with Vaccine-Induced Antigen-Binding Hotspots  
731 Develop Broad HIV Neutralization. *Cell* **178**, 567-584.e519 (2019).
- 732 29. B. Nogal *et al.*, HIV envelope trimer-elicited autologous neutralizing antibodies bind a  
733 region overlapping the N332 glycan supersite. *Science Advances* **6**, eaba0512 (2020).
- 734 30. M. G. Pauthner *et al.*, Vaccine-Induced Protection from Homologous Tier 2 SHIV  
735 Challenge in Nonhuman Primates Depends on Serum-Neutralizing Antibody Titers.  
736 *Immunity* **50**, 241-252.e246 (2019).
- 737 31. A. P. West, Jr. *et al.*, Structural Insights on the Role of Antibodies in HIV-1 Vaccine and  
738 Therapy. *Cell* **156**, 633-648 (2014).
- 739 32. D. Sok, D. R. Burton, Recent progress in broadly neutralizing antibodies to HIV. *Nat*  
740 *Immunol* **19**, 1179-1188 (2018).
- 741 33. J. Huang *et al.*, Identification of a CD4-Binding-Site Antibody to HIV that Evolved Near-  
742 Pan Neutralization Breadth. *Immunity* **45**, 1108-1121 (2016).
- 743 34. P. Schommers *et al.*, Restriction of HIV-1 Escape by a Highly Broad and Potent  
744 Neutralizing Antibody. *Cell* **180**, 471-489 e422 (2020).
- 745 35. T. Zhou *et al.*, Structural basis for broad and potent neutralization of HIV-1 by antibody  
746 VRC01. *Science* **329**, 811-817 (2010).
- 747 36. A. P. West, Jr., R. Diskin, M. C. Nussenzweig, P. J. Bjorkman, Structural basis for  
748 germline gene usage of a potent class of antibodies targeting the CD4 binding site of  
749 HIV-1 gp120. *Proc Natl Acad Sci U S A Plus* **109**, E2083-2090 (2012).

- 750 37. J. G. Jardine *et al.*, Minimally Mutated HIV-1 Broadly Neutralizing Antibodies to Guide  
751 Reductionist Vaccine Design. *PLoS Pathog* **12**, e1005815 (2016).
- 752 38. J. Umotoy *et al.*, Rapid and Focused Maturation of a VRC01-Class HIV Broadly  
753 Neutralizing Antibody Lineage Involves Both Binding and Accommodation of the N276-  
754 Glycan. *Immunity* **51**, 141-154 e146 (2019).
- 755 39. R. W. Sanders *et al.*, A next-generation cleaved, soluble HIV-1 Env Trimer, BG505  
756 SOSIP.664 gp140, expresses multiple epitopes for broadly neutralizing but not non-  
757 neutralizing antibodies. *PLoS Pathog* **9**, e1003618 (2013).
- 758 40. H. I. V. C. S. International *et al.*, The major genetic determinants of HIV-1 control affect  
759 HLA class I peptide presentation. *Science* **330**, 1551-1557 (2010).
- 760 41. J. F. Scheid *et al.*, Sequence and Structural Convergence of Broad and Potent HIV  
761 Antibodies That Mimic CD4 Binding. *Science* **333**, 1633-1637 (2011).
- 762 42. N. A. Doria-Rose *et al.*, Mapping Polyclonal HIV-1 Antibody Responses via Next-  
763 Generation Neutralization Fingerprinting. *PLoS Pathog* **13**, e1006148 (2017).
- 764 43. J. F. Scheid *et al.*, Sequence and Structural Convergence of Broad and Potent HIV  
765 Antibodies That Mimic CD4 Binding. *Science*, (2011).
- 766 44. T. Schoofs *et al.*, Broad and Potent Neutralizing Antibodies Recognize the Silent Face of  
767 the HIV Envelope. *Immunity* **50**, 1513-1529 e1519 (2019).
- 768 45. A. deCamp *et al.*, Global panel of HIV-1 Env reference strains for standardized  
769 assessments of vaccine-elicited neutralizing antibodies. *Journal of virology* **88**, 2489-  
770 2507 (2014).
- 771 46. B. F. Haynes *et al.*, Cardiolipin polyspecific autoreactivity in two broadly neutralizing  
772 HIV-1 antibodies. *Science* **308**, 1906-1908 (2005).
- 773 47. L. Scharf *et al.*, Structural basis for germline antibody recognition of HIV-1  
774 immunogens. *Elife* **5**, (2016).
- 775 48. R. Derking *et al.*, Enhancing glycan occupancy of soluble HIV-1 envelope trimers to  
776 mimic the native viral spike. *Cell reports* **35**, 108933 (2021).
- 777 49. Y. Gavel, G. von Heijne, Sequence differences between glycosylated and non-  
778 glycosylated Asn-X-Thr/Ser acceptor sites: implications for protein engineering. *Protein*  
779 *Eng* **3**, 433-442 (1990).
- 780 50. Q. Liu *et al.*, Quaternary contact in the initial interaction of CD4 with the HIV-1  
781 envelope trimer. *Nature structural & molecular biology* **24**, 370-378 (2017).
- 782 51. W. D. Tolbert, D. N. Nguyen, Z. R. Tehrani, M. M. Sajadi, M. Pazgier, Near-Pan-  
783 neutralizing, Plasma Deconvoluted Antibody N49P6 Mimics Host Receptor CD4 in Its  
784 Quaternary Interactions with the HIV-1 Envelope Trimer. *mBio* **12**, e0127421 (2021).
- 785 52. Q. Liu *et al.*, Improvement of antibody functionality by structure-guided paratope  
786 engraftment. *Nature Communications* **10**, (2019).
- 787 53. G. B. Stewart-Jones *et al.*, Trimeric HIV-1-Env Structures Define Glycan Shields from  
788 Clades A, B, and G. *Cell* **165**, 813-826 (2016).
- 789 54. C. Havenar-Daughton *et al.*, The human naive B cell repertoire contains distinct  
790 subclasses for a germline-targeting HIV-1 vaccine immunogen. *Science translational*  
791 *medicine* **10**, (2018).
- 792 55. J. Jardine *et al.*, Rational HIV immunogen design to target specific germline B cell  
793 receptors. *Science* **340**, 711-716 (2013).
- 794 56. J. G. Jardine *et al.*, HIV-1 broadly neutralizing antibody precursor B cells revealed by  
795 germline-targeting immunogen. *Science* **351**, 1458-1463 (2016).

- 796 57. M. M. Sajadi *et al.*, Identification of Near-Pan-neutralizing Antibodies against HIV-1 by  
797 Deconvolution of Plasma Humoral Responses. *Cell* **173**, 1783-1795 e1714 (2018).
- 798 58. R. Diskin *et al.*, Increasing the potency and breadth of an HIV antibody by using  
799 structure-based rational design. *Science* **334**, 1289-1293 (2011).
- 800 59. P. D. Kwong *et al.*, Structure of an HIV gp120 envelope glycoprotein in complex with  
801 the CD4 receptor and a neutralizing human antibody. *Nature* **393**, 648-659 (1998).
- 802 60. R. S. Rudicell *et al.*, Enhanced potency of a broadly neutralizing HIV-1 antibody in vitro  
803 improves protection against lentiviral infection in vivo. *Journal of virology* **88**, 12669-  
804 12682 (2014).
- 805 61. T. Zhou *et al.*, Multidonor analysis reveals structural elements, genetic determinants, and  
806 maturation pathway for HIV-1 neutralization by VRC01-class antibodies. *Immunity* **39**,  
807 245-258 (2013).
- 808 62. S. A. Sievers, L. Scharf, A. P. West, Jr., P. J. Bjorkman, Antibody engineering for  
809 increased potency, breadth and half-life. *Curr Opin HIV AIDS* **10**, 151-159 (2015).
- 810 63. I. Hotzel *et al.*, A strategy for risk mitigation of antibodies with fast clearance. *mAbs* **4**,  
811 753-760 (2012).
- 812 64. K. J. Bar *et al.*, Effect of HIV Antibody VRC01 on Viral Rebound after Treatment  
813 Interruption. *N Engl J Med* **375**, 2037-2050 (2016).
- 814 65. L. Corey *et al.*, Two Randomized Trials of Neutralizing Antibodies to Prevent HIV-1  
815 Acquisition. *N Engl J Med* **384**, 1003-1014 (2021).
- 816 66. R. M. Lynch *et al.*, HIV-1 fitness cost associated with escape from the VRC01 class of  
817 CD4 binding site neutralizing antibodies. *Journal of virology* **89**, 4201-4213 (2015).
- 818 67. T. Schoofs *et al.*, HIV-1 therapy with monoclonal antibody 3BNC117 elicits host  
819 immune responses against HIV-1. *Science* **352**, 997-1001 (2016).
- 820 68. P. D. Kwong, J. R. Mascola, HIV-1 Vaccines Based on Antibody Identification, B Cell  
821 Ontogeny, and Epitope Structure. *Immunity* **48**, 855-871 (2018).
- 822 69. K. M. Roskin *et al.*, Aberrant B cell repertoire selection associated with HIV neutralizing  
823 antibody breadth. *Nat Immunol* **21**, 199-209 (2020).
- 824 70. N. A. Doria-Rose, E. Landais, Coevolution of HIV-1 and broadly neutralizing antibodies.  
825 *Curr Opin HIV AIDS* **14**, 286-293 (2019).
- 826 71. T. Zhou *et al.*, Structural Repertoire of HIV-1-Neutralizing Antibodies Targeting the  
827 CD4 Supersite in 14 Donors. *Cell* **161**, 1280-1292 (2015).
- 828 72. M. Sarzotti-Kelsoe *et al.*, Optimization and validation of the TZM-bl assay for  
829 standardized assessments of neutralizing antibodies against HIV-1. *J Immunol Methods*  
830 **409**, 131-146 (2014).
- 831 73. A. P. West, Jr. *et al.*, Computational analysis of anti-HIV-1 antibody neutralization panel  
832 data to identify potential functional epitope residues. *Proceedings of the National*  
833 *Academy of Sciences of the United States of America* **110**, 10598-10603 (2013).
- 834 74. I. S. Georgiev *et al.*, Delineating antibody recognition in polyclonal sera from patterns of  
835 HIV-1 isolate neutralization. *Science* **340**, 751-756 (2013).
- 836 75. J. F. Scheid *et al.*, A method for identification of HIV gp140 binding memory B cells in  
837 human blood. *J Immunol Methods* **343**, 65-67 (2009).
- 838 76. D. Sok *et al.*, Recombinant HIV envelope trimer selects for quaternary-dependent  
839 antibodies targeting the trimer apex. *Proceedings of the National Academy of Sciences of*  
840 *the United States of America* **111**, 17624-17629 (2014).

- 841 77. P. Pugach *et al.*, A native-like SOSIP.664 trimer based on an HIV-1 subtype B env gene.  
842 *Journal of virology* **89**, 3380-3395 (2015).
- 843 78. T. Tiller *et al.*, Efficient generation of monoclonal antibodies from single human B cells  
844 by single cell RT-PCR and expression vector cloning. *J Immunol Methods* **329**, 112-124  
845 (2008).
- 846 79. L. von Boehmer *et al.*, Sequencing and cloning of antigen-specific antibodies from  
847 mouse memory B cells. *Nature protocols* **11**, 1908-1923 (2016).
- 848 80. M. P. Lefranc *et al.*, IMGT, the international ImMunoGeneTics information system.  
849 *Nucleic Acids Res* **37**, D1006-1012 (2009).
- 850 81. E. Traggiai *et al.*, Development of a human adaptive immune system in cord blood cell-  
851 transplanted mice. *Science* **304**, 104-107 (2004).
- 852 82. J. A. Horwitz *et al.*, HIV-1 suppression and durable control by combining single broadly  
853 neutralizing antibodies and antiretroviral drugs in humanized mice. *Proceedings of the*  
854 *National Academy of Sciences of the United States of America* **110**, 16538-16543 (2013).
- 855 83. Y. J. Zhang *et al.*, Envelope-dependent, cyclophilin-independent effects of  
856 glycosaminoglycans on human immunodeficiency virus type 1 attachment and infection.  
857 *Journal of virology* **76**, 6332-6343 (2002).
- 858 84. M. Caskey *et al.*, Antibody 10-1074 suppresses viremia in HIV-1-infected individuals.  
859 *Nat Med* **23**, 185-191 (2017).
- 860 85. B. F. Keele *et al.*, Identification and characterization of transmitted and early founder  
861 virus envelopes in primary HIV-1 infection. *Proceedings of the National Academy of*  
862 *Sciences of the United States of America* **105**, 7552-7557 (2008).
- 863 86. J. F. Salazar-Gonzalez *et al.*, Deciphering human immunodeficiency virus type 1  
864 transmission and early envelope diversification by single-genome amplification and  
865 sequencing. *Journal of virology* **82**, 3952-3970 (2008).
- 866 87. N. P. Chung *et al.*, Stable 293 T and CHO cell lines expressing cleaved, stable HIV-1  
867 envelope glycoprotein trimers for structural and vaccine studies. *Retrovirology* **11**, 33  
868 (2014).
- 869 88. L. Scharf *et al.*, Broadly Neutralizing Antibody 8ANC195 Recognizes Closed and Open  
870 States of HIV-1 Env. *Cell* **162**, 1379-1390 (2015).
- 871 89. W. Kabsch, XDS. *Acta Crystallogr D Biol Crystallogr* **66**, 125-132 (2010).
- 872 90. M. D. Winn *et al.*, Overview of the CCP4 suite and current developments. *Acta*  
873 *Crystallogr D Biol Crystallogr* **67**, 235-242 (2011).
- 874 91. A. J. McCoy *et al.*, Phaser crystallographic software. *J Appl Crystallogr* **40**, 658-674  
875 (2007).
- 876 92. P. D. Adams *et al.*, PHENIX: a comprehensive Python-based system for macromolecular  
877 structure solution. *Acta Crystallogr D Biol Crystallogr* **66**, 213-221 (2010).
- 878 93. P. Emsley, B. Lohkamp, W. G. Scott, K. Cowtan, Features and development of Coot.  
879 *Acta Crystallogr D Biol Crystallogr* **66**, 486-501 (2010).
- 880 94. D. N. Mastrorade, Automated electron microscope tomography using robust prediction  
881 of specimen movements. *J Struct Biol* **152**, 36-51 (2005).
- 882 95. J. Zivanov *et al.*, New tools for automated high-resolution cryo-EM structure  
883 determination in RELION-3. *Elife* **7**, (2018).
- 884 96. K. Zhang, Gctf: Real-time CTF determination and correction. *J Struct Biol* **193**, 1-12  
885 (2016).

- 886 97. A. Punjani, J. L. Rubinstein, D. J. Fleet, M. A. Brubaker, cryoSPARC: algorithms for  
887 rapid unsupervised cryo-EM structure determination. *Nat Methods* **14**, 290-296 (2017).
- 888 98. J. M. Bell, M. Chen, P. R. Baldwin, S. J. Ludtke, High resolution single particle  
889 refinement in EMAN2.1. *Methods* **100**, 25-34 (2016).
- 890 99. T. D. Goddard, C. C. Huang, T. E. Ferrin, Visualizing density maps with UCSF Chimera.  
891 *J Struct Biol* **157**, 281-287 (2007).
- 892 100. V. B. Chen *et al.*, MolProbity: all-atom structure validation for macromolecular  
893 crystallography. *Acta Crystallogr D Biol Crystallogr* **66**, 12-21 (2010).
- 894 101. J. Agirre *et al.*, Privateer: software for the conformational validation of carbohydrate  
895 structures. *Nat Struct Mol Biol* **22**, 833-834 (2015).
- 896 102. S. Unni *et al.*, Web servers and services for electrostatics calculations with APBS and  
897 PDB2PQR. *J Comput Chem* **32**, 1488-1491 (2011).
- 898 103. E. Krissinel, K. Henrick, Inference of macromolecular assemblies from crystalline state.  
899 *Journal of molecular biology* **372**, 774-797 (2007).
- 900
- 901

## 902 **Acknowledgments**

903 We thank members of the Bjorkman, Nussenzweig and Klein labs for helpful discussions. B-cell  
904 sorting of donor 391370 was performed with help of Kristie Gordon and Gaëlle Breton.  
905 Neutralization fingerprinting analysis was performed by Ivelin Georgiev. Sequencing analysis of  
906 antibody sequences and patient plasma env genes was supported by Joy Pai. BG505 SOSIP.664-  
907 Avi, the CHO cell lines expressing the BG505 SOSIP.664 v4.1 trimer and DU422 SOSIP.664 v4.1  
908 trimer, and the BG505.T332N gp160 expression plasmid were kind gifts of Albert Cupo, John P.  
909 Moore and Rogier W. Sanders. We thank Dr. Jost Vielmetter, Pauline Hoffman, and other  
910 members of the Protein Expression Center in the Beckman Institute at Caltech for expression  
911 assistance. Structural studies were assisted by the Caltech Molecular Observatory (Dr. Jens Kaiser,  
912 director) and the Biological and Cryogenic Transmission Electron Microscopy Center at Caltech  
913 (Drs. Andrey Malyutin and Songye Chen, directors). This work was supported by the National  
914 Institute of Allergy and Infectious Diseases of the National Institutes of Health Grant HIVRAD  
915 P01 AI100148 (to P.J.B. and M.C.N.), National Institutes of Health Grant NIH P50 AI150464 (to  
916 P.J.B.), the Bill and Melinda Gates Foundation Collaboration for AIDS Vaccine Discovery Grants  
917 OPP1124068 (to M.C.N. and P.J.B.) and 1146996 (M.S.S.), NIH Center for HIV/AIDS Vaccine  
918 Immunology and Immunogen Discovery (CHAVI-ID) 1UM1 AI100663-01 (M.C.N.), the  
919 European Research Council (ERC-StG639961) (F.K.), the German Center for Infection Research  
920 (DZIF) (F.K.). C.O.B was supported by the Hanna Gray Fellowship Program from the Howard  
921 Hughes Medical Institute and the Postdoctoral Enrichment Program from the Burroughs Wellcome  
922 Fund. T.S. was supported by the Ernst Jung Career Advancement Award for Medical Research,  
923 grant UL1 TR001866 from the National Center for Advancing Translational Sciences (NCATS,  
924 NIH Clinical and Translational Science Award (CTSA) program), and DZIF grant TI 07.002. We

925 thank the Gordon and Betty Moore and Beckman Foundations for gifts to Caltech to support the  
926 Molecular Observatory and electron microscopy. M.C.N. and B.D.W. are HHMI investigators.

927

### 928 **Author Contributions:**

929 C.O.B., T.S., M.C.N., and P.J.B., conceived the study. T.S. and J.G. performed B-cell sorting and  
930 antibody cloning of BG24 family members. C.O.B., Y.E.L., N.S-T., and K.E.H-T, performed  
931 protein purification and structural studies. P.N.P.G., K.E.H-T., A.P.W., and C.O.B., performed *in*  
932 *vitro* 12-strain neutralization assays on engineered BG24 constructs and analyzed the data. C.O.B.,  
933 and N.S-T., conducted structural studies. T.S. and H.G. performed antibody *in vivo* experiments.  
934 P.S. conducted neutralization assays on viral mutants and envelope sequencing from mouse  
935 plasma. J.C.C.L. and T.S. conducted env sequencing from patient plasma. M.S.S. carried out  
936 neutralization testing on the 126-virus cross-clade panel. J.F.S. and M.S.S. conducted plasma  
937 screening of HIV controller cohort. A.P.T. and B.D.W. collected and provided patient samples  
938 from the HIV controller cohort. C.O.B., T.S., M.C.N., and P.J.B., wrote the manuscript with  
939 contribution from all authors.

940

### 941 **Competing Interests**

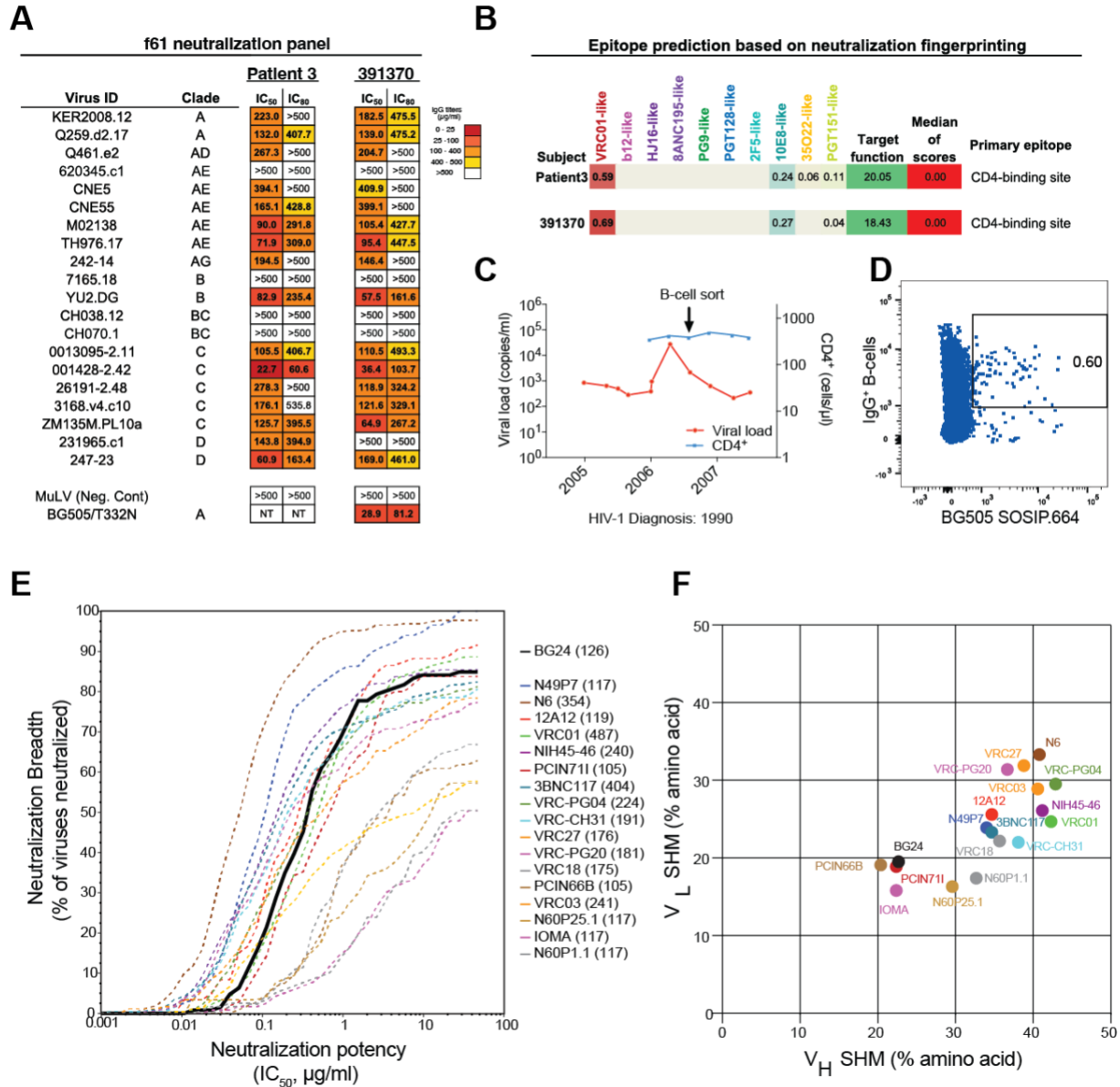
942 The Rockefeller University has filed a provisional patent application in connection with this work  
943 on which C.O.B., T.S., M.C.N., and P.J.B. are inventors. All other authors declare they have no  
944 competing interests.

945

### 946 **Data and materials availability**

947 Nucleotide sequences of BG24 antibody family members and plasma env sequences from subject  
948 391370 have been deposited in GenBank (Accession Numbers XXX-XXX). The atomic models  
949 of the unliganded BG24<sub>S60A</sub> Fab and BG24-BG505–10-1074 complex have been deposited in the  
950 Protein Data Bank (PDB; <http://www.rcsb.org/>) under accession codes PDB 7UCE and 7UCF,  
951 respectively. Coordinates for the atomic model and cryo-EM map generated from cryo-EM studies  
952 of the BG24<sub>CDR2-v2</sub>-DU422-101074 complex has been deposited at the PDB and the Electron  
953 Microscopy Databank (EMDB, <http://www.emdataresource.org/>) under codes PDB 7UCG and  
954 EMD-26443, respectively. All data are available in the main text or the supplementary materials.  
955

956 **Figures and Tables**



957

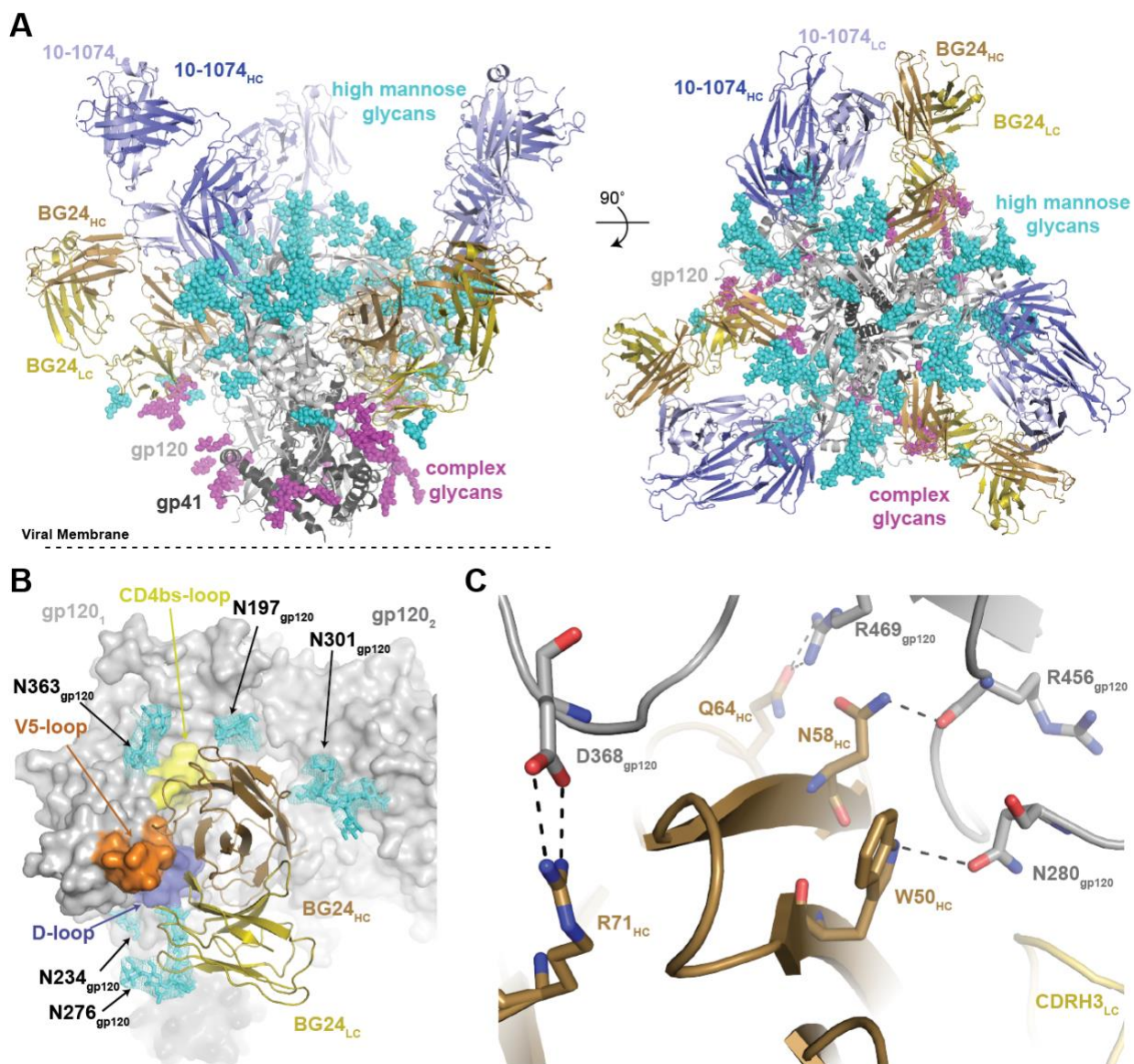
958 **Fig. 1. Isolation and characterization of antibody BG24 from donor 391370.**

959 A) Neutralization data of donor 391370's serum IgG against a 20-virus fingerprinting panel (f61).

960 The average median inhibitory concentrations (IC<sub>50</sub>) in µg/mL are shown from duplicate  
 961 neutralization measurements.

962 B) Fingerprinting analysis of f61 serum neutralization for Patient 3 and donor 391370.

- 963 C) Plasma viral load and peripheral blood CD4<sup>+</sup> T cell counts of donor 391370 over time. The  
964 arrow indicates the time point for BG505 SOSIP.664 bait-sorting.
- 965 D) Sorting of single BG505 SOSIP.664<sup>+</sup> IgG<sup>+</sup> memory B-cells.
- 966 E) Neutralization breadth and potency of BG24 on a 126-virus cross clade panel. Neutralization  
967 testing performed in duplicates, average shown.
- 968 F) Somatic hypermutation (SHM) analysis of VRC01-like bNAbs, shown as % amino acid  
969 changes relative to germline variable gene sequence.
- 970
- 971



972

973 **Fig. 2. BG24 recognition of HIV-1 Env has features in common with VRC01-class bNAb.**

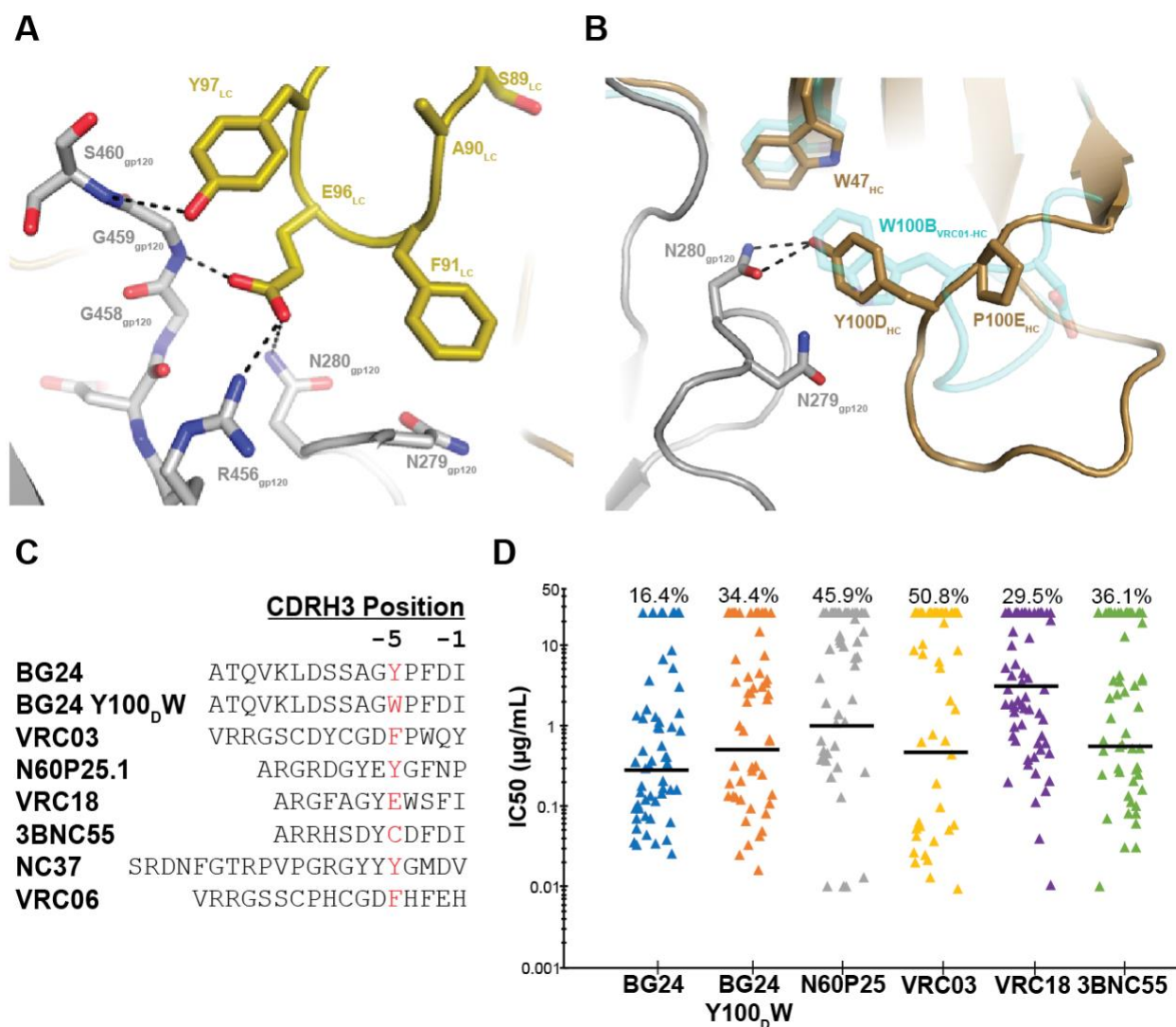
974 A) Side and top views of the 3.9 Å X-ray structure of the BG24-BG505-10-1074 complex colored  
975 by components (dark gray, gp41; light gray, gp120; shades of blue, 10-1074 Fab; shades of  
976 brown, BG24 Fab).

977 B) Surface representation of gp120 (gray), with main loops at the CD4bs colored (yellow, CD4bs-  
978 loop; blue, D-loop; orange, V5-loop) and BG24 shown as cartoon representation. N-linked

979 glycans modeled in the structure are shown as cyan sticks with electron density contoured at  
980  $1.5\sigma$ .

981 C) Stick representation of residue level contacts between VRC01-class signature residues in  
982 BG24<sub>HC</sub> (brown) with gp120 (gray). Dashed black lines indicated potential for H-bond  
983 interactions.

984



985

986 **Fig. 3. BG24's CDR3 sequence motifs are uncommon among VRC01-like bNAbs.**

987 A) Stick representation of residue level contacts between residues in BG24's CDRL3 loop

988 (yellow) with gp120 (gray). Potential H-bond interactions are shown as black dashed lines.

989 VRC01 CDRH3 is also shown in **panel B** (cyan).

990 B) Stick representation of residue level contacts between residues in BG24's CDRH3 loop

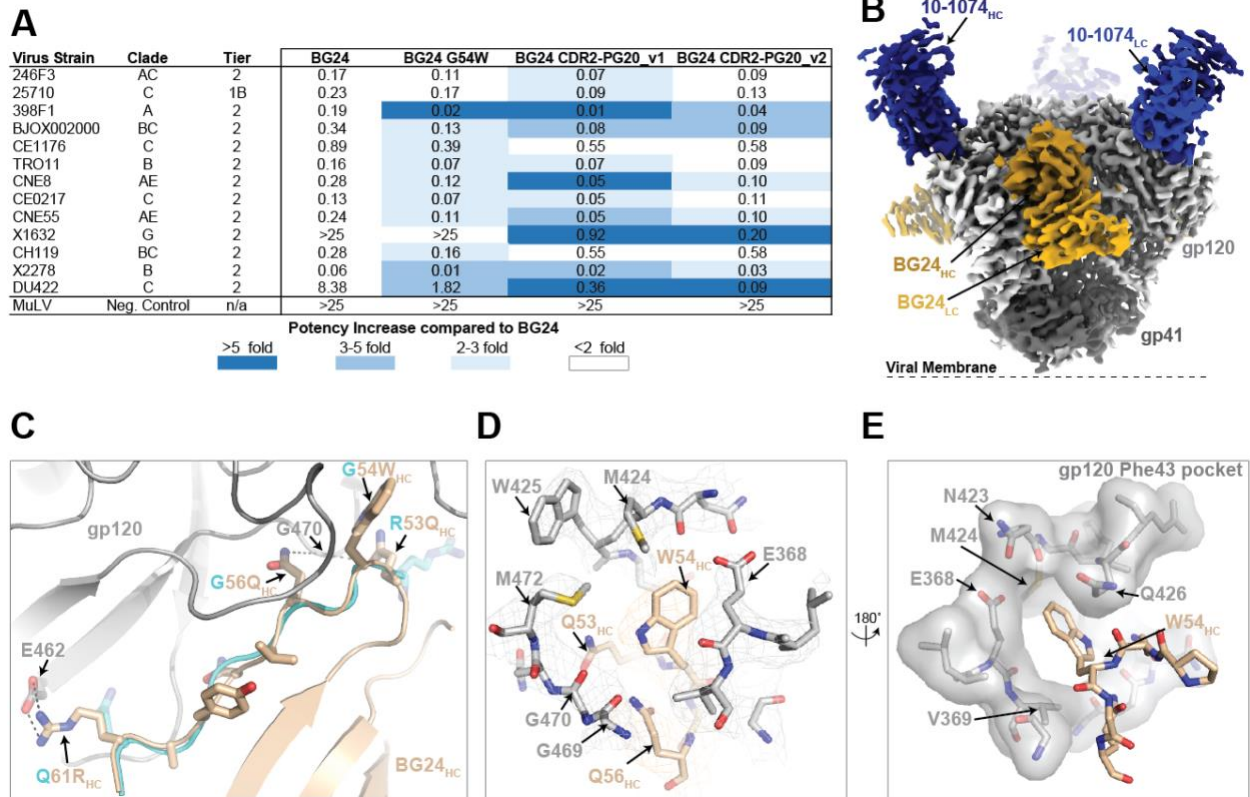
991 (brown) with gp120 (gray). The CDRH3 loop of VRC01 (PDB 6VX8) is also shown (cyan).

992 Potential H-bond interactions are shown as black dashed lines.

993 C) CDRH3 sequence alignment of VRC01-like antibodies that lack a Trp residue at the -5  
994 position.

995 D) Neutralization data for in-common (n=61) cross-clade viruses of BG24 and VRC01-like  
996 antibodies that lack a Trp residue at the -5 position. The geometric mean IC<sub>50</sub> value against  
997 antibody-sensitive strains is indicated by the horizontal black line. The percentage of non-  
998 neutralized strains is indicated on the top for each antibody. Analysis of neutralization and  
999 graphing was done using the Antibody Database (v 2.0) (73).

1000



1001

1002 **Fig. 4. Improvements to BG24 neutralization potency and breadth.**

1003 A) Neutralization data of engineered BG24 constructs against the global 12 virus panel. The  
 1004 average mean IC<sub>50</sub> in µg/mL are shown from duplicate neutralization measurements.

1005 B) Side and top views of the 3.5Å single-particle cryo-EM reconstruction of the BG24<sub>PG20</sub>-CDR2-  
 1006 v2-DU422-10-1074 complex colored by components (dark gray, gp41; light gray, gp120;  
 1007 shades of blue, 10-1074 Fab; shades of brown, BG24 Fab)

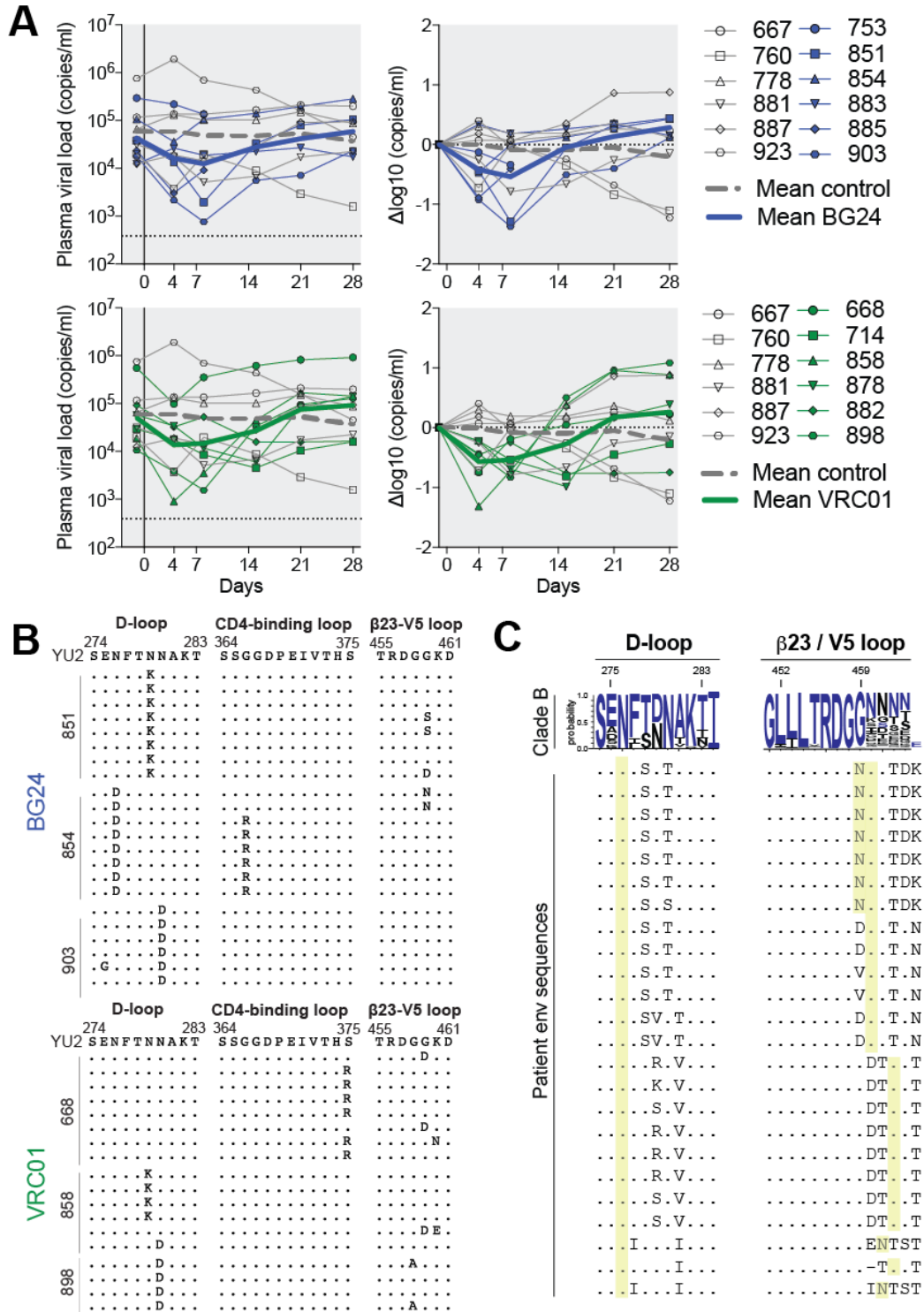
1008 C) Cartoon and stick representation of BG24<sub>PG20</sub>-CDR2-v2 CDRH2 (wheat) at the gp120 (gray)  
 1009 interface. The CDRH2 loop from the BG24-BG505 complex (cyan) is overlaid with amino  
 1010 acid mutations between the two constructs labeled. Potential H-bond interactions are shown  
 1011 as black dashed lines.

1012 D) Modeling of the Phe43 gp120 pocket with BG24<sub>G54W</sub> pocket-filling mutation highlighted  
 1013 (wheat). Electron density contoured at 7σ is shown for gp120 and BG24.

1014 E) Surface representation of gp120 Phe43 pocket (gray) and BG24<sub>G54W</sub> pocket-filling mutation

1015 (wheat).

1016



1017

1018 **Fig. 5. BG24 has comparable *in vivo* efficacy to VRC01 in HIV<sub>YU2</sub>-infected humanized mice.**

1019 A) Antibody monotherapy of humanized mice infected with HIV<sub>YU2</sub>. Left graphs show  
1020 absolute viremia (y-axis) in mice treated with antibody monotherapy (BG24, n=6, dark  
1021 blue; VRC01, n=6, dark green) or untreated control mice (n = 6, grey) over the course of  
1022 the experiment (x axis, days). Right graphs show relative log drop after initiation of  
1023 antibody therapy ( $\Delta\log_{10}$  copies/mL). Thick blue/green and thick dashed gray lines  
1024 indicate the mean viral load of treated and untreated mice, respectively. Mice were infected  
1025 3 weeks prior to therapy initiation and received 1 mg of IgG as a loading dose followed by  
1026 twice-weekly administration of 0.5 mg for 3 weeks. The dotted line at the bottom indicates  
1027 the limit of accuracy of the qPCR assay (384 copies/mL). Data from one experiment.

1028 B) Plasma HIV-1 Env sequences obtained 4 weeks after initiation of therapy from mice treated  
1029 with BG24 (top) and VRC01 (bottom), respectively. Letters show amino acid mutations  
1030 relative to the HIV<sub>YU2</sub> molecular clone. Residues numbered according to HIV-1<sub>HXB2</sub>.

1031 C) HIV-1 Env sequences obtained from donor plasma RNA. Letters indicate amino acid  
1032 mutations compared with consensus clade B (blue letters) shown on top. Black letters in  
1033 the consensus sequence indicate amino acids also observed at each position with lower  
1034 frequencies. Yellow columns indicate potential N-linked glycosylation sites (PNGSs).  
1035 Residues are numbered according to HIV-1<sub>HXB2</sub>.

1036



- 1039 A) Sequence alignment of BG24 and BG24 minimally-mutated constructs with germline  
1040 sequences. Somatic mutations compared to germline are shown with BG24 paratope residues  
1041 derived from SHM shown as red. Complete paratope is labeled below sequence alignment.
- 1042 B) Paratope residues from germline V genes (green), somatic mutation (red) and CDR3 loops  
1043 (orange) are shown as sticks on BG24.
- 1044 C-F) Representative mutations that increase contacts of mature BG24 with CD4bs. Model of  
1045 germline BG24 (pink) was superposed with the BG24-BG505-101074 structure.
- 1046 F) Neutralization data of engineered minimally-mutated BG24 constructs against the global 12-  
1047 strain viral panel. The average mean  $IC_{50}$ s in  $\mu\text{g/mL}$  are shown from duplicate neutralization  
1048 measurements.